Review article **Open Access**

Thomas G. Mayerhöfer* and Jürgen Popp

Periodic array-based substrates for surface-enhanced infrared spectroscopy

DOI 10.1515/nanoph-2017-0005
Received January 9, 2017; revised April 25, 2017; accepted May 5, 2017

Abstract: At the beginning of the 1980s, the first reports of surface-enhanced infrared spectroscopy (SEIRS) surfaced. Probably due to signal-enhancement factors of only 10^1 to 10^3, which are modest compared to those of surface-enhanced Raman spectroscopy (SERS), SEIRS did not reach the same significance up to date. However, taking the compared to Raman scattering much larger cross-sections of infrared absorptions and the enhancement factors together, SEIRS reaches about the same sensitivity for molecular species on a surface in terms of the cross-sections as SERS and, due to the complementary nature of both techniques, can valuably augment information gained by SERS. For the first 20 years since its discovery, SEIRS relied completely on metal island films, fabricated by either vapor or electrochemical deposition. The resulting films showed a strong variance concerning their structure, which was essentially random. Therefore, the increase in the corresponding signal-enhancement factors of these structures stagnated in the last years. In the very same years, however, the development of periodic array-based substrates helped SEIRS to gather momentum. This development was supported by technological progress concerning electromagnetic field solvers, which help to understand plasmonic properties and allow targeted design. In addition, the strong progress concerning modern fabrication methods allowed to implement these designs into practice. The aim of this contribution is to critically review the development of these engineered surfaces for SEIRS, to compare the different approaches with regard to their performance where possible, and report further gain of knowledge around and in relation to these structures.

Keywords: surface-enhanced infrared spectroscopy; plasmonics; sensing; periodic array-based substrates; metamaterials.

1 Introduction

The discovery of surface-enhanced infrared spectroscopy (SEIRS) is usually associated with the paper of Hartstein, Kirtley, and Tsang entitled "Enhancement of the Infrared Absorption from Molecular Monolayers with Thin Metal Overlayers" [1]. In this paper, the authors accordingly claim "the first observation" of this effect. Based on their experimental findings, they calculated an enhancement factor of 10^4 compared to conventional transmission experiments and speculate about the origin of the enhancement as being "due to collective electron resonances" excited by the incident light. These collective electron resonances are, nowadays, well known and usually called plasmon-polaritons or, simply, plasmons.

Using finely grained metals as catalytic substrates and investigating the adsorbance of molecules, in particular gases, by infrared spectroscopy, has a long tradition and goes back at least 25 years more than the official discovery of SEIRS (see, e.g. [2]). Effects like anomalous transmission or dispersion were sometimes reported ([3] and references therein), but not systematically investigated.

The magnitude of the signal enhancement (i.e. the transmittance or reflectance signal generated by the analyte, ratioed to a reference signal and scaled to the number of molecules of this analyte, which we will call enhancement factor in the following) that is attainable with metal island films has, since the official discovery, been carefully examined. Its limits are usually stated, somewhat more conservatively, as within 10^1 to 10^2. In other cases, factors up to 10^3 can be found [the calculation of enhancement factors is, for reasons that will be discussed later in more detail, even more arguable than in the case of surface-enhanced Raman spectroscopy (SERS)]

***Corresponding author: Thomas G. Mayerhöfer,** Leibniz Institute of Photonic Technology (IPHT), Albert-Einstein-Str. 9, D-07745 Jena, Germany; and Institute of Physical Chemistry and Abbe Center of Photonics, Friedrich Schiller University, Helmholtzweg 4, D-07743 Jena, Germany, e-mail: Thomas.Mayerhoefer@uni-jena.de
Jürgen Popp: Leibniz Institute of Photonic Technology (IPHT), Albert-Einstein-Str. 9, D-07745 Jena, Germany; and Institute of Physical Chemistry and Abbe Center of Photonics, Friedrich Schiller University, Helmholtzweg 4, D-07743 Jena, Germany

[4–6]. The mechanism(s) behind this signal enhancement gave reason for many speculations. Typically, effective medium theories [7–10] have been successfully used to explain the optical properties of metal island films. These theories can only describe the macroscopic properties, but are able to give semi-quantitative insight into underlying microscopic mechanisms, e.g. they can explain the change of band shapes and intensities, thereby, allowing to predict, to a certain, extent signal enhancements and optimal SEIRS conditions [11, 12]. However, they do not provide local field or intensity distributions, a prerequisite for improving SEIRS performance [13]. Some progress was made by investigating the dependence of properties from the size of the metal particles by varying the nominal thickness of the films. When this size increases, isolated particles begin to grow until they tend to approach each other (this limit is called the percolation threshold) and, eventually, form continuous films. It can be observed that during this process, the signal of analytes attached to the structures strongly grow until they reach a maximum. This maximum is reached close to or at the percolation threshold. Afterward, the signal rapidly decreases with further increase in the nominal thickness and completely vanishes as soon as a continuous film is formed [14–16]. With increasing signal, unfortunately, the band shapes in the spectra of the analytes begin to change. While they resemble that of the bands of the imaginary part of the complex refractive index at lower enhancement, they generally become more distorted around the percolation threshold and finally resemble the real part of the refractive index [16, 17].

Fifteen years ago the last paragraph of a review of surface-enhanced infrared absorption (SEIRA, a term used synonymous to SEIRS) authored by Masatoshi Osawa started with the following sentences [5]: “Despite twenty years of history, SEIRA has received less attention than SERS. This is probably due to the smaller enhancement factor of SEIRA.” This statement is still valid. However, an important factor in arriving at this statement might be that the metal island films that were nearly exclusively used until less than 10 years ago could only be optimized to a certain degree. Mostly, as we know today, the enhancement of these plasmonic substrates is based on an off-resonance enhancement mechanism, which naturally has its limits, while SERS profits mostly from an on-resonance mechanism. For resonant plasmonic enhancement to occur in the infrared spectral range, structure sizes are needed that cannot be reached with metal island films as they become continuous before. The solution to this problem is to use other methods of fabrication, which start with continuous films and shape structures out of those. Such top-down approaches [18] gained in importance in the last decade as they allow to sculpt substrates in a desired and very reproducible way. Usually, such substrates consist of arrays of structures, i.e. particles or holes. Together with numerical methods to simulate the optical properties of such periodic structures, it is now possible to investigate a large variety of shapes and their benefit for SEIRS in a methodical and systematic way. It is the goal of this work to review the corresponding substrates with regard to their benefits and advantages as far as this is possible. In order to be able to evaluate the performance of these sculptured array films, we first start with a section detailing the enhancement mechanisms that are in play in the case of SEIRS substrates and with a discussion of the calculation of enhancement factors that are often provided for new structures together with numerical simulations of the near-field enhancement $|E|/|E_0|$ or the near-field intensity enhancement $|E|^2/|E_0|^2$. We will also detail why it is usually hard to compare enhancement factors from different systems. Afterward, we will start with particle-based substrates and discuss merits and disadvantages of the different shapes. Compared to hole-based substrates, the former clearly outnumber the latter, but hole-based substrates show some very interesting properties and have some particular advantages. Particle and hole-based substrates have in common that they are usually carved out of a single metallic layer, which is placed on a dielectric material that acts mostly as supporting structure. In contrast, in the last couple of years, a more complex structure consisting of at least two metallic layers separated by a dielectric, of which only the metallic layer at the top is structured while the bottom layer acts as a mirror, gains in importance. These perfect absorber structures can provide higher enhancements and are increasingly used as SEIRS substrates. In the last section, which concludes this review, we will pool and discuss some approaches that are also plasmonic in nature, but not metal-based.

2 Theory

2.1 Enhancement mechanisms

The goal of this section is to make the reader familiar with the latest findings about the mechanisms behind SEIRS in order to be able to better compare the different substrates and their benefits. It is generally accepted that there are three main contributions to the signal enhancement, which can be first differentiated by their origin and categorized as “chemical” and “physical” enhancement.

The physical enhancement can be subdivided depending on if the plasmon frequency is matched with the vibrational frequencies of the analyte (which we call the on-resonance contribution) or if the plasmon frequency is far off, and there is seemingly little direct interaction between plasmons and vibrations. The latter is usually the case for metal island films. As already mentioned in the Introduction, metal island films show their strongest signal enhancement close to the percolation threshold. At this threshold, the sizes of the particles usually are still in the 100 nm range [16], which would put their plasmon resonance well in the NIR spectral range when isolated.

The role of the chemical enhancement is still not very well understood. Generally, it is assumed that chemical bonding leads to changes in the electronic structure of the molecule, while physical adsorption does not. An interesting example in this respect is the activation of N_2 in the presence of Ni. While N_2, due to the lack of a dipole moment change during its vibration, does not show a vibrational band in the infrared spectrum, it becomes infrared active when adsorbed on finely grained Ni. The corresponding mode has an infrared absorption cross section in the order of 10^{-18} cm^2 [19], which is amazingly large, lies between the typical values for fluorescence (10^{-16} cm^2) and infrared absorption cross sections (10^{-20} cm^2) [20] and gives rise to the assumption that enhancement is at play. It was suspected that N_2 might not be chemisorbed, but that a strong polarization leads to a non-zero vibrational transition moment (a sharp distinction between these two cases might be just as meaningful and clear as the one between ionic and heteropolar bonding). In general, there have been no new insights into the mechanism of chemical enhancement, so it might still be valid to assume that its contribution to SEIRS is of minor importance in comparison with SERS [21]. Accordingly, we will concentrate on effects concerning which new insights were gained in the last years and, in particular, in connection with sculpted substrates. Nevertheless, for completeness, we just mention some additional effects that affect intensities and were mentioned in literature, such as orientational order [14] (in contrast to randomly oriented molecules in solution or in pellets, an up to threefold increase is anticipated) and an improved geometry by nanostructuring, which makes the surface-bound receptors more accessible and increases the surface area [22].

2.1.1 On-resonance enhancement

As already stated, one big advantage of the use of top-down approaches to fabricate substrates for plasmon-enhanced sensing, in general, is that these fabrication methods allow tailoring the substrates in a way that the enhancement is optimized for a certain spectroscopic method at hand. However, as these fabrication methods, like electron beam lithography (which is, of course, only one step of a sometimes very complex fabrication process), are relatively expensive and time consuming, it is advisable to design the structures beforehand and to be able to see how a change of certain parameters influences the performance of the substrate. Luckily, a number of numerical methods have been developed to help in evaluating this performance beforehand like the finite difference time domain (FDTD) method, the finite element method (FEM), and the method of moments (MoM) or boundary element method (BEM) to name just a few.

It was noticed early, that the band shapes of analytes are altered when they interact with metals (see, e.g. [3]), an effect that was called anomalous transmission. Indeed, in the case of the metal island films, this effect increases with the enhancement factor of the structure. However, it does not only persist when the enhancement already begins to decrease, but even seems to increase [16]. While weak absorption bands are nearly symmetrical, they tend to become asymmetrical, and the shapes seem to be a mixture of the typical symmetric form of the bands in the imaginary part of the refractive index spectrum (for low oscillator strengths) and the asymmetrical band shapes of the real part of the refractive index function ("dispersion like"). Finally, they can completely take on this "dispersion-like" form [17], which is also called and described as "Fano-like" [23].

Such band shapes are not unknown in spectroscopy, in general. They occur when two processes interact, one of which has, e.g. a continuum-like or broad spectral nature, while the spectral feature of the second is narrower. Based on the work of Langreth [24], it was speculated that the line shape, in the case of metal island films, is caused by the interaction of "an isolated vibrational mode of an atom or molecule adsorbed on a metallic surface in the presence of electron-hole damping", an interaction that belongs to the realm of the chemical enhancement. For substrates with a plasmon resonance tailored to the vibrational mode of an adsorbed molecule, a more natural explanation is to employ the interaction of the usually broad plasmonic band and the narrow vibrational band of the analyte. An important step toward a quantitative description of this interaction marked the paper of Giannini et al. [25]. In this paper a formula was derived that allowed a more or less parameter-free approach to understand the spectral changes that the vibrational band undergoes when the plasmon resonance is gradually tuned to match the

resonance frequency of the vibrational band. As long as the difference in resonance frequency between both oscillators is comparably large, the band caused by the vibration of the molecule is comparably weak but symmetric. Its height begins to increase with decreasing difference, the band takes on the typical Fano-like band shape until the oscillator frequencies match, and a symmetric shape is recovered. Interestingly, the band is then often inverted, which means that the broad band shows a symmetric dip, which mimics a feature known from the quantum interference effects and is called "electromagnetically induced transparency" (EIT). Giannini et al. showed that their model can also be successfully applied to model the asymmetric band features of so-called dolmen structures where two plasmonic resonances interact. Both cases, plasmon-analyte interaction as well as the plasmon-plasmon interaction, have a bright resonance (the dipolar plasmon resonance) and a (relatively) dark resonance (molecular vibration or, e.g. a quadrupole mode) in common. These modes are coupled, and an energy transfer takes place from the bright to the dark mode, which influences the band shapes of both.

Some more insight into the nature of this coupling between bright and dark mode is provided by the work of Adato et al. [26]. By applying the model of two coupled oscillators, the authors are able to show that not only electromagnetically induced transparency but also absorption enhancement (electromagnetically induced absorption, EIA) can take place in coupled molecular and plasmonic resonators. Accordingly, not only dips can occur when the resonance frequencies match, but also an additional narrow ascent. Using an approach from transmission line theory known as temporal coupled-mode theory (TCMT), the loss of the bright mode is subdivided in radiative ($\triangleq$ scattering) and intrinsic loss ($\triangleq$ absorption), and the ratio of these two loss mechanisms (more precisely the ratio between the radiative and intrinsic damping constants γ_{Ae}/γ_{A0}) is shown to be the dominating factor influencing the band shape of the plasmon and the vibrational resonance in absorption. If the ratio is smaller/larger than one, the system is called under-/overcoupled and a dip/additional ascent results, i.e. EIT/EIA. In the presence of a molecule, the plasmon couples to a molecular vibration, and the damping rate of this vibration enhances via coupling the intrinsic damping rate. A system that is slightly overcoupled can be driven by this additional intrinsic damping to a system that is undercoupled. Interestingly, if the addition of the molecular damping leads to a situation where the ratio between the radiative and intrinsic damping rate is close to unity (a situation that is called critical coupling), then the absorption band of the plasmon is left nearly unchanged, i.e. neither dip nor ascent occurs, a situation which is very important for so-called perfect absorbers (see Section 3.3). We have used the oscillator model from Ref. [26] to calculate the corresponding band shapes also for situations where the frequencies of plasmon and molecular vibration do not agree. In particular, we assume the situation of a thin molecular film placed on a perfect absorber consisting of a metal antenna placed on top of a dielectric film above a continuous metallic film, which resembles that presented in Ref. [26]. Assuming time harmonic fields, the mode amplitude of the plasmonic mode A is given by:

$$j\omega A = j\omega_A A - (\gamma_{A0} + \gamma_{Ae})A - \gamma_\mu A + j\omega_\mu A + \kappa s_+ \tag{1}$$

with the effective damping constant $\gamma_\mu = \mu^2\gamma_P/[(\omega-\omega_P)^2+\gamma_P^2]$ and the effective frequency shift $\omega_\mu = \mu^2(\omega-\omega_P)/[(\omega-\omega_P)^2+\gamma_P^2]$. The second oscillator, which is the dark mode, e.g. a molecular vibration, is labeled by P. Accordingly, ω, ω_A, and ω_P are the frequency, the resonance frequency of the first resonator (the plasmon), and the resonance frequency of the second resonator (the molecular vibration). The damping constant of this second resonator is given by γ_P. Further variables are the coupling constant μ (a measure of the interaction between plasmon and vibrational mode), the coupling rate of the incident wave κ, and the wave amplitude of the incoming wave s_+. It is important to note that the mode amplitude and the traveling wave amplitude are normalized in a way to yield the energy stored in the resonance ($|A|^2$) and the power carried by the wave ($|s_+|^2$), respectively. Not presented in Ref. [26] is the way how to calculate the absorbance $Abs.$ (which is equal to $1-R$, wherein R is the reflectance as we assume a single port system and, therefore, the transmittance $T=0$) of the coupled system, which can be found after some algebra to be

$$Abs. = \frac{4\gamma_{Ae}(\gamma_{A0}+\gamma_\mu)}{(\omega-\omega_A-\omega_\mu)^2+(\gamma_{A0}+\gamma_{Ae}+\gamma_\mu)^2}. \tag{2}$$

The perfect absorber structures, in particular, the metal-insulator-metal structures introduced in more detail in Chapter 3.3.1 are perfect test cases as, on the one hand, the continuous metal layer assures that $T\approx 0$, and on the other hand, it is possible to vary the ratio between scattering and absorption [26]. While absorption is usually not directly measurable (with a few exceptions, e.g. photoacoustic infrared spectroscopy), reflectance is. We, therefore, present in Figure 1 reflectance curves to demonstrate the influence on the radiative and intrinsic damping constants.

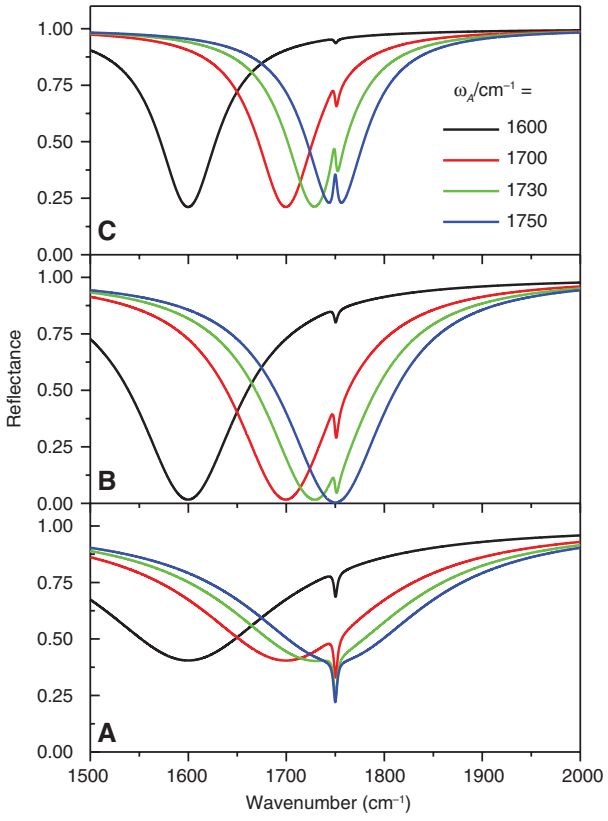

Figure 1: Reflectance due to the coupled system plasmon-molecular vibration for varying resonance frequencies of the plasmon ω_A (1600, 1700, 1730, and 1750 cm^{-1}) and $\omega_P = 1750\ cm^{-1}$, $\gamma_P = 2\ cm^{-1}$, $\mu_P = 5\ cm^{-1}$. (A) Depicts an overcoupled situation with $\gamma_{Ae}/\gamma_{A0} = 90/20$, whereas the ratio $\gamma_{Ae}/\gamma_{A0} = 35/27$ leads to critical coupling due to the interaction with the dark oscillator (B) and $\gamma_{Ae}/\gamma_{A0} = 10/50$ to undercoupling (C).

It is quite interesting to observe that in situations where overcoupling is assumed $\gamma_{Ae}/(\gamma_{A0}+\gamma_P) > 1$ (Figure 1A), the model correctly predicts broader plasmon bands due to stronger scattering, an ascent if plasmon and vibrational resonance have the same frequency, as well as a stronger signal of the molecular vibration even if plasmon and vibrational frequency are detuned. For critical coupling [$\gamma_{Ae}/(\gamma_{A0}+\gamma_P) = 1$], a molecular signal can no longer be detected if plasmon and vibrational resonance have the same frequency [Figure 1B, note that in our example, the values for the damping constants still lead to slight overcoupling, but the deviation from $\gamma_{Ae}/(\gamma_{A0}+\gamma_P) = 1$ is too small to be noticeable]. For undercoupling $\gamma_{Ae}/(\gamma_{A0}+\gamma_P) < 1$, comparably narrow plasmon resonances occur, and for $\omega_A = \omega_P$, a dip results.

From comparable findings, Adato et al. [26] conclude that in the case of resonant SEIRS, "…what is observed or measured in these applications is the perturbation of the plasmonic resonance by the (molecular) absorber…". Furthermore, "…the magnitude of this feature (EIA or EIT), and therefore the success of the plasmonic structure design, does not necessarily scale with the standard field enhancement metric." As a consequence, it might be advisable to use the above-mentioned numerical tools like FDTD, etc., not only to design structures with the highest enhancement but also to investigate the ratio between the radiative and intrinsic damping rate of the plasmonic structure, at least if absorption dominates. In addition, it seems to be important to investigate the optical properties after "adding" a suitable analyte (given its dielectric function is known) and inspecting the magnitude of the spectral changes after the addition.

The importance of scattering for signal enhancement was investigated by Neuman et al. [27], on the example of linear plasmonic antennas, the structure, which was most extensively studied up to now. As one of the results, the authors come to the conclusion "… that the ratio between the antenna's scattering losses and intrinsic losses is an important design parameter to consider for the hosting antennas which can be tuned to optimize the SEIRA performance" which completely agrees with the finding in Ref. [26] where this principle was demonstrated and formulated as $C_{sca}/C_{abs} = \gamma_{Ae}/\gamma_{A0}$ with C_{sca} being the scattering and C_{abs} the absorption cross sections, respectively. It must be mentioned, however, that in the case of analytes with weak oscillators, the design recommendation of the plasmonic antenna $\gamma_{Ae}/\gamma_{A0} = 1$ presents a challenge as small fabrication issues can lead to the situation where $\gamma_{Ae}/(\gamma_{A0}+\gamma_P) \approx 1$ with vanishing absorption signals.

Neuman et al. calculated explicitly the contributions of scattering and absorption to the extinction cross section of linear nanoantennas, which is quite instructive to examine in detail. In Figure 2, the individual cross sections are displayed for 10 nm-thick layers of analytes on three different linear nanoantennas, the dimensions of which are chosen in a way that they mostly absorb, which show nearly equal absorption and scattering cross sections or mostly scatter. The normalized signal contrast increases by about 25% if the system antenna plus monolayer shows about equal contributions from absorption and scattering, while the whole signal contrast virtually stems from the scattering, and absorption does not contribute, which agrees with the results presented in Ref. [26] and Figure 1.

Obviously, TCMT is not able to account for far-field scattering. Further weaknesses of TCMT are that it cannot predict plasmon band shifts due to the change of the refractive index of the sample, and as it is based on perturbation theory, it also cannot account for changes in the oscillator frequencies of the plasmon and the molecular

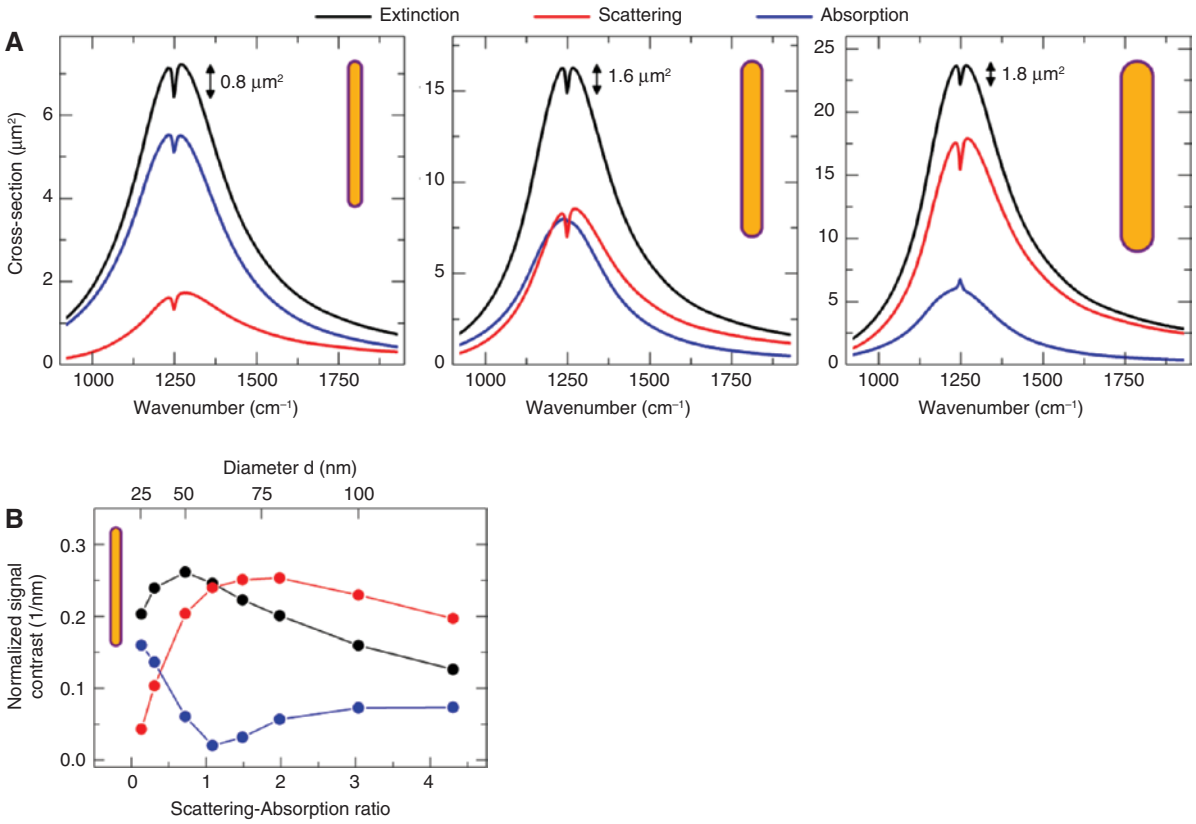

Figure 2: (A) Absorption, scattering, and extinction cross-section spectra of a dominantly absorbing antenna (left, d = 35 nm, l = 2.45 µm), a larger antenna with scattering approximately equal to absorption (middle, d = 60 nm, l = 2.97 µm), and an antenna that dominantly scatters (right, d = 100 nm, l = 3.2 µm). The resonance frequency of the hosting antennas is kept at approximately 1250 cm^{-1}. The sample is a dielectric layer homogeneously covering the antenna surface (thickness t = 10 nm). (B) Vibrational signal contrast in the absorption, scattering, and extinction cross-section spectra (normalized to the volume of the dielectric layer) versus the ratio between plasmonic scattering and absorption for fixed plasmonic resonance frequency and varying volume of the hosting antenna. Adapted with permission from Ref. [27]. Copyright 2015 American Chemical Society.

vibration due to coupling. In addition, TCMT predicts that the maximum far-field signal should coincide with the oscillator positions, something which has been shown to be incorrect (see below). On the other hand, reflectance as calculated by TCMT is readily compared to the experiment, while extinction cross sections are not (this might not be obvious, but extinction, better called attenuance as recommended by the IUPAC, is usually defined as $A \equiv -\lg T$. This definition is generally not compatible with Maxwell's equations and, therefore, with extinction or attenuance as derived from microscopic theories. This point will be explained in more detail in Section 2.2). It would, therefore, be important to investigate the contributions of scattering and absorption to the (specular) reflectance and transmittance, the quantities that are generally measured for systems that include analytes.

A further interesting finding of Neuman et al. [27] is that near-field scattering leads to having a considerable part of electric field polarized perpendicular to the long axis of the antennas and parallel to the substrate surface in the vicinity of the antennas. The authors show this on the example of an analyte material with cubic crystal symmetry. It would be interesting, in this regard, how this depolarization influences the spectra of anisotropic layers of analytes, as monolayers often show lower symmetry due to ordering effects. Generally, it would be interesting to learn how the spectral response is influenced by shape, i.e. if the findings of Neuman et al. [27] are generally applicable for all shapes of antennas.

Before we continue with the non-resonant enhancement, we want to point out two further peculiarities in connection with resonant enhancement. The first is the fact that the wavenumber of a plasmonic resonance extracted from far-field measurements (assuming that a maximum or minimum in a spectrum equals this wavenumber) usually differs from the position of the highest enhancement by up to 100 cm^{-1} [28]. This difference is, as Vogt et al. point out, probably insignificant in the few cases of

comparably broad molecular vibrational bands, like for the amide bands or for N-H and, in particular, O-H stretching vibrations, but may play an increasingly important role for bands with much smaller widths than plasmon bands, which essentially applies to all other vibrational bands of organic molecules. The reason for this red shift can be explained by simply applying a harmonic oscillator model to the plasmon excitation [29] (accordingly, comparable red shifts exist for phonons, which can also be modeled by harmonic oscillators and have high oscillator strengths). In this respect, it is instructive to note that upon loading the plasmonic structure with an analyte, a red shift of the plasmon band maximum (in absorption) in the far field is observed. This red shift has a very similar order of magnitude as the red shift between maximum near-field enhancement and the derived oscillator position from the maximum of the far-field spectrum (also in absorption). Again, such shifts remind of the shifts that are observed for phonon bands of materials measured in powdered form in pellets with matrix materials (the higher the real part of the index of refraction of the matrix material, the stronger the red shift). It is generally important to keep in mind that the positions of the band maxima in the far-field spectra rarely indicate oscillator frequencies except if the oscillators are very weak or for randomly oriented polycrystalline materials with optically small crystallites where orientational averaging is at play. The oscillator frequencies usually stay fixed, even if the matrix changes and induces a spectral shift of the bands in the spectra [28, 30].

What is rarely mentioned in literature is that a markedly higher enhancement of the electric field also persists comparably far off the plasmonic resonance. This is also reflected in the aforementioned oscillator model, which predicts even at much lower or higher frequencies than the frequency of the plasmon a non-negligible energy transfer from the bright to the dark mode when the equations provided in Ref. [26] are used. In light of this finding, it may sometimes not be a simple task to differentiate between on-resonance and off-resonance enhancement.

2.1.2 Off-resonance enhancement

A very well-known off-resonance enhancement mechanism is the lightning rod effect, according to which the electric field is enhanced at tips or spikes due to a higher surface charge density, which leads to "large (electric) field components perpendicular to the boundaries" [31], which was initially shown on the example of ellipsoids [32]. Vibrational nanospectroscopic methods like tip-enhanced Raman scattering (TERS) and scattering-type scanning near-field optical microscopy (s-SNOM) employ this effect to record vibrational spectra with nanometric resolution [33–35]. The lightning rod effect can be further enhanced if two tips or spikes are brought in close vicinity to each other along their long axes so that a nanometric gap between these two objects is formed because of near-field coupling of these objects (gap effect).

Such gap effects can also occur in the case of the gap structures in metallic films even when the particles grow larger in diameter than the uncovered substrate regions and, correspondingly, the lightning rod effect vanishes. The overall reflectance and transmittance signal enhancements of vibrational modes of molecules due to these gaps were modeled with effective medium theories, which allow to treat these random structures. In the last years, the optical properties of metal island films could be mimicked with two different approaches that, in a strict sense, do not belong to the topic of this review, but helped to gain valuable insight in the enhancement mechanisms, which is why we will shortly introduce the corresponding results.

In the first paper, Le et al. introduced metallic nanoparticle arrays, which can serve both as SERS and as SEIRS substrates [36]. The characteristic of these substrates, which were fabricated by applying a drop of nanoshell solution onto a substrate and letting the solvent evaporate, are "characterized by two features, a relatively sharp resonance in the NIR and a very broad, continuum-like resonance in the MIR". The sharp feature resembles very much the quadrupolar plasmon resonance of the isolated nanoshells, while the broad resonance originates from the dipolar plasmon resonance, which strongly red shifts and broadens due to coupling with the dipolar plasmon resonances of neighbored nanoshells. The resulting on-resonance enhancement is intermingled with off-resonance enhancement, which results from the fact that, at comparably low frequencies, metals tend toward being perfect conductors, which expel any electric field. Therefore, the field is concentrated in the gaps.

In contrast, Shimada et al. investigated systematically the enhancement of periodic gold square column arrays on silicon [37]. The substrates were fabricated by electron beam lithography. However, as the dimensions of the square columns were not tuned toward resonance, the paper lies somewhat outside the focus of this review. The edge lengths of these squares were varied from 100 nm to 350 nm, and the pitches from 200 nm to 650 nm to mimic the growth of the islands of metal island films with increasing nominal thickness. The maximum size of 350 nm and below, as well as gap sizes not below 100 nm ensured that the enhancement effects were off-resonance.

The authors could show that the magnitude of the electric field inside the gaps is a function of the ratio of gap size and edge length.

2.2 Enhancement factors

Reviewing the application of SERS for bioanalysis, Larmour and Graham refrained from citing or comparing enhancement factors [38]. We agree with their reasoning that there are many assumptions that are incorporated in such calculations that lead to enhancement factors. Indeed, by just comparing the pure numbers, one could gain the impression that the performances of similar structures vary by 3 to 4 orders of magnitude. How is this possible? One important factor to consider is that often enhancement factors are given as averages, while for sculpted nanoantennas, it is more common that signals are normalized against the number of molecules in the hotspot. Note first that there is no consistent definition of what to understand by a hotspot. Kleinmann et al. defined a hotspot with regard to SERS as "a junction or close interaction of two or more plasmonic objects where at least one object has a small radius of curvature on the nm scale" [39]. This definition would, in particular, exclude single plasmonic antennas from having a hotspot. Therefore, in the following, we will use the term hotspot generally in connection with the volume(s) in which enhanced electric fields around one plasmonic object exist, as this is usually the case in literature concerning SEIRS. We realize, however, that this is still not a precise or quantitative definition, as for such a definition, we would need to define a threshold or cut-off value of the electric field or the field intensity at which the corresponding point in space would be considered as belonging to the boundary, which encloses the volume of the hotspot. While it is possible by numerical methods like FDTD and FEM to calculate the electric near fields around a plasmonic object, in principle, and interesting progress has been made to measure these values directly or indirectly [40–42] an agreement about such a threshold value does not exist. From the calculated electric fields, it is possible to define a near-field enhancement factor $|E|/|E_0|$ or a near-field intensity enhancement factor $|E|^2/|E_0|^2$ which can offer some insights into signal enhancement as absorption is proportional to $(\boldsymbol{\mu}\cdot\mathbf{E})^2$, where $\boldsymbol{\mu}$ is the transition dipole moment, and the other factor is determined by the near field. The numerical methods are all based in some way on the idea of solving Maxwell's equations numerically, which is more flexible and needs much less effort than finding analytical solutions for a given structure (if such a solution exists at all). As for their nature, these numerical methods provide accurate results with regard to optical properties like reflectance and transmittance of a given structure and with respect to the enhancements of the electric and magnetic fields. Eventually, with increasing numerical effort, e.g. the number of points in FDTD and FEM, at which Maxwell's equations are solved (i.e. decreasing the size of the mesh), the solutions of the different methods converge, which is an indication that a stable and reliable solution has been found (for further information, see, e.g. [43–45]). The agreement between experiment and modeled property then only depends on (on the side of the numerical modeling) how reliable the dielectric functions of the materials used for a substrate are known in the spectral regions of interest. While these methods are very powerful, the amount of time needed may be a limiting factor. In addition, these methods are usually not able to provide insights into the mechanism of the spectral enhancement. However, as already stated, they allow to calculate a near-field enhancement of a certain structure in hotspots, as shown in Figure 2, which can be used to estimate the signal enhancement.

One point that we want to mention in this respect is that the electric near-field enhancement is sometimes calculated without analyte in place. As can be seen in Figure 3, the presence of analyte generally lowers the near field and the near-field intensity in dependence of its optical properties. If the analyte does not occupy the complete volume of the hotspot, the near field tends to increase again somewhat with the onset of empty space after it has decreased exponentially inside the analyte, at least in the case of slits.

For the determination of experimental, i.e. signal enhancement factors, several influencing variables have to be taken into account as the number and distribution of molecules or formula units of the analyte within the hotspot, and, the particular vibrational mode that is used and its oscillator strength. With regard to analytes employed to test the performance of a certain structure or substrate a large variety exists, which can be divided mainly into two groups. To the first group belong chemisorbed molecules, which indeed chemically bind to the surface of the plasmonic object. One of the most common analytes belonging to this group is octadecanethiol (ODT), which binds to gold via its thiol group. If the substrate is carefully rinsed after incubation in a solution of ODT, only monolayers remain on exposed gold surfaces. A typical representative of the second group is poly-methyl-methacrylate (PMMA), which does not bind to the plasmonic object when deposited, which also means that it forms continuous films covering the whole surface of a substrate. Therefore, most of the analyte is outside of hotspots, but

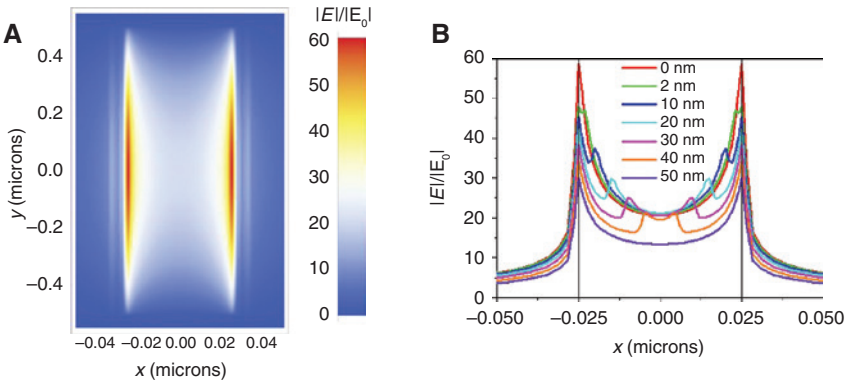

Figure 3: (A) Near-field enhancement map of an empty slit with a width of 50 nm and a length of 1000 nm at its bottom calculated by a FDTD simulation. (B) Near-field enhancement cross section at $y=0$ of an empty (0 nm), partly filled (analyte layer thickness between 2×2 nm and 2×20 nm), and completely filled slit (50 nm). The analyte layers are placed at the sidewalls at $x=-0.025$ and $x=0.025$ μm, which are indicated by the two maxima from which the fields decay exponentially toward the center of the slit at $x=0$. The interfaces between layer and empty slit are revealed by a comparably weak but steep rise of the field, which, correspondingly, is absent for the empty and completely filled slits.

can contribute to the overall measured reflectance or transmittance signal. Generally, it might be more useful to use the first group to evaluate the performance of substrates that aim, if not for single molecule sensitivity, at a sensitivity/spectral signal as high as possible with as few molecules as feasible. In combination with a controlled deposition of analytes into the hotspots, these substrates have the prospect to investigate or identify very small sample amounts. This is not much different from the situation in SERS, except that SEIRS is still several orders of magnitude away from single molecule sensitivity.

What is, however, very different in the case of SERS and SEIRS, or in the case of Raman and infrared spectroscopy, in general, is that, in contrast to Raman spectroscopy, the actual signal measured in infrared spectroscopy is not directly proportional to the number of molecules or the concentration of the vibrating species.

Infrared spectroscopy is, nowadays (and already since some time), a routinely applied and common technique. What is somewhat surprisingly less common, is the awareness or even the knowledge that it is not absorbance or extinction [both terms are often used synonymous due to the fact that both are often calculated by the same equations; see Eqs. (3) and (4) below] that is actually measured, but transmittance or reflectance instead (i.e. it is the ratio of the number of photons with and without the sample in place that is determined). Commercially available spectrometers, nowadays, routinely convert transmittance T or reflectance R into absorbance. In the case of a transmittance measurement, the *transmittance absorbance* A is calculated according to:

$$-\log T = \mathrm{A}. \tag{3}$$

The equality sign is usually not justified, as this equation is not compatible with Maxwell's equations, and the resulting errors can be as large as one order of magnitude, in particular, in the case of strongly reflecting materials [46] (alternatively, the equation must be seen as a mere defining equation). The missing compatibility can readily be deduced from Eq. (3) in combination with the Beer-Lambert law, according to which absorption is proportional to the imaginary part of the refractive index, but is independent of its real part. Correspondingly, in the textbooks of optics, the transmittance through a slab of a material, which can be characterized by a scalar dielectric function, is described by either Airy's formulas or Abelès' formalism. The Beer-Lambert law is part of this formalism to describe the *propagation* within a medium, but this law alone cannot account for the multiple reflections inside the slab. The frequency dependence of the complex index of refraction eventually leads to different distance waves of different frequencies that can travel inside the slab due to multiple reflection. This in consequence leads to the failure of Eq. (3) (if additional scattering plays a role, further approximations obscure the relation between the via transmittance "measured extinction" and the extinction cross sections, calculated, e.g. via FDTD simulations, even more [47]).

In particular, for the transmittance of plasmonic substrates, if loaded with analyte or not, due to the high reflectance of the metallic areas, compatibility of Eq. (3) with Maxwell's equations is improbable, but has yet to be explored. Often the absorbance of an analyte on a plasmonic substrate is compared with that without substrate for the calculation of enhancement factors. The same is true if the absorbance or attenuance is defined as:

$$-\log\frac{R}{R_0} \equiv \mathrm{A}. \tag{4}$$

Here, R is the reflectance of the loaded substrate, and R_0 is the reflectance of the substrate without analyte. In the original literature [48], this absorbance is called *reflectance absorbance* to emphasize that the so-calculated or so-defined absorbance or attenuance cannot be directly compared with *transmittance absorbance* (except if very strict conditions hold, such as an attenuated total reflection experiment is carried out, and the oscillator strength is so low that its imaginary index of refraction is lower than 0.01 [48]). As a detailed investigation of the compatibility of Eq. (4) to Maxwell's equations is still missing (besides the fact that Eq. (3) and Eq. (4) are not generally compatible to each other, there is, further strong indication that this compatibility is non-existing, like, e.g. the proof of non-adherence to linearity as provided in the chapter "Infrared Spectrometry of Thick Organic Films on Metallic Substrates" of Ref. [49]), it is safe to assume that also caution is necessary if the calculation of enhancement factors is based on this equation.

In practice, as the use of absorbance or attenuance can easily introduce undeterminable errors of the order of one magnitude or more, one has to revert to the comparison of either the reflectance and/or transmittance signals. Comparing these quantities obtained with a certain SEIRS active structure and those measured with reference methods on the same vibrational mode taking into account the differing number of area or volume that is probed or the different number of molecules inside the probed volume, a potential definition of an (signal) enhancement factor *ef* can be the following:

$$ef = \frac{I_{\mathrm{Ex}}}{I_{\mathrm{Ref}}} \cdot \frac{N_{\mathrm{Ref}}}{N_{\mathrm{Ex}}}. \tag{5}$$

Here, I_{Ex} represents the experimental reflectance or transmittance of the SEIRS-active structure, and N_{Ex} is the number of molecules probed inside the hotspot and I_{Ref} and N_{Ref} the corresponding quantities for the reference experiments. According to this definition, a careful choice of the reference experiment is necessary. To illustrate this fact, it is helpful to compare transmittance and reflectance spectra of one representative of each of the above two groups (ODT and PMMA) using different IR-spectroscopic techniques.

In the case of ODT, we choose to employ a monolayer and for PMMA, a 30 nm-thick layer. Unfortunately, ODT optical constants are not available in the literature. However, polyethylene (PE) is known to have a very similar spectrum, even when non-oriented, except for the missing CH_3 groups, but this is of minor importance in the following considerations. The ODT monolayers are known to have a thickness of about 2–2.8 nm [50, 51]. While it is not possible to fabricate and measure in transmittance such thin free-standing films, we can use the optical constants of PE [52] and PMMA [53] together with Abelès formalism to calculate their transmittance and reflectance assuming that the layers are isotropic, i.e. with randomly oriented transition moments, but can be characterized by a scalar dielectric function. In Figure 4, we show the results for a 2 nm-thick PE film and a 30 nm-thick PMMA film in transmission as free-standing film and on KBr, in reflectance (angle of incidence $\alpha = 80°$, parallel polarized light as well as for $\alpha = 20°$ and non-polarized light) on gold and in reflectance (angle of incidence 0°) on a 500 nm-thick SiO_2 layer on gold.

For PE, the strongest band caused by the asymmetric CH_2 stretching vibration at 2921 cm^{-1} gives rise to a transmission decrease of about 0.4% for a 2 nm-thick film, which is with about 0.3% somewhat lower if the film is placed on a 100-µm-thick plate of KBr. The corresponding infrared reflection absorption (IRRAS) signal of PE on gold is at $\alpha = 80°$ and parallel polarized light with about 1.5% nearly four times larger compared to that of the free-standing film on the expense of the need for a more complex accessory (experimental values for ODT range between 0.3% [54] and 1% [55]). These measurement conditions are used to generate reference values for the calculation of enhancement factors of metal island films. If $\alpha = 20°$ and non-polarized light is used, which resemble possible measurement conditions for IR-microscopes that are sometimes employed in the SEIRS literature in connection with arrays of sculpted nanoantennas, the signal decreases to 0.02%. For the 30 nm-thick PMMA film, we find a transmittance signal of 3.4% for the C=O stretching vibration at 1732 cm^{-1} for the free-standing film, which is lowered to 2.6% if the film would be placed on the KBr plate. The reflectance signals for the IRRAS conditions amount to 11.8% ($\alpha = 80°$, parallel polarized) and 0.4% ($\alpha = 20°$, non-polarized). In particular, the results for the IRRAS calculations demonstrate that the choice of the conditions for the reference experiment in terms of angle of incidence and polarization can alter enhancement factors defined along Eq. (5) easily by 2 to 3 orders of magnitude. A very important physical reason for this finding is the fact that the electric field at the interface of a perfect conductor is forced to have only a component perpendicular to the interface. For large angles of incidence and parallel (p-) polarized light, the polarization direction of the incoming light is mostly oriented parallel to the interface.

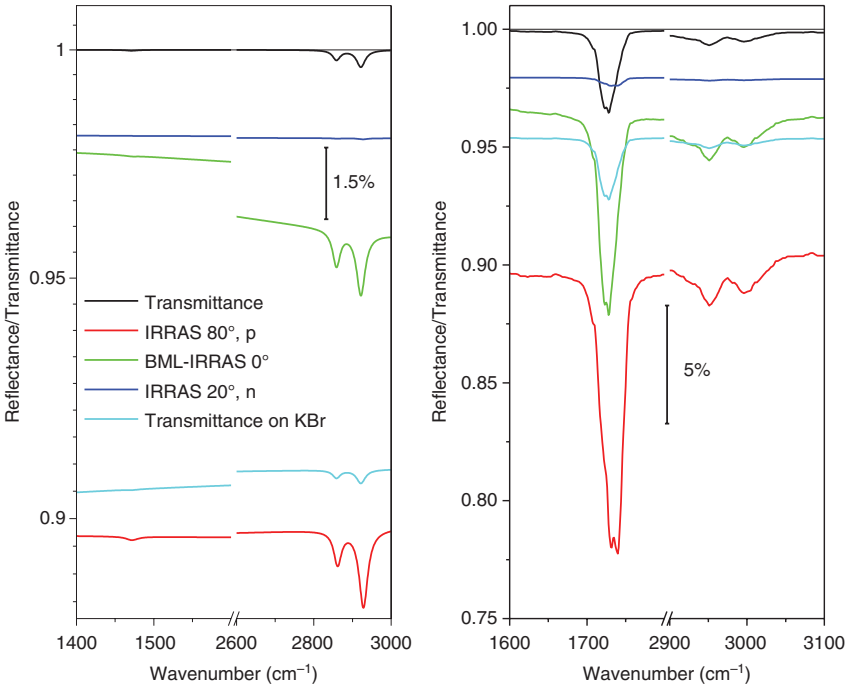

Figure 4: Comparison of the signal strength of 2 nm-thick PE (left) and 30 nm-thick PMMA (right) in the form of a free-standing film in transmittance (black curve), on KBr in transmittance (turquoise curve), on gold with an angle of incidence of 80° and parallel polarization in reflectance (red curve), on gold with an angle of incidence of 20° and non-polarized radiation (blue curve) and on a 500 nm (PE) and 700 nm (PMMA)-thick SiO_2 layer on gold with normal incidence in reflectance (green curve). All spectra are calculated based on the respective optical constants and Abelès formalism.

For small angles of incidence, however, the incident light is mostly polarized perpendicular to the surface of the metal. Most nanoantennas are investigated with these conditions. However, nanoantennas usually have surfaces oriented perpendicular to the interface of the substrate on which they are placed, and those are often the ones generating the hotspots and contributing most strongly to the SEIRS signals, which could serve as an argument to use IRRAS experiments with angles of incidence >60° as reference experiments [56].

While we have used exact formulas to calculate transmittance and reflectance of the PE and PMMA layers, for monolayers, approximate formulas are available in literature [57, 58]. Sometimes it is not possible to obtain a certain reference spectrum experimentally, e.g. ODT does not bind to most dielectrics. One possible way to obtain reference values is to analyze IRRAS spectra by dispersion analysis [59] as carried out, e.g. in Ref. [60] or with the use of inverse dielectric function modeling [61], which is of particular advantage in the case of parallel polarized radiation and large angles of incidence. In this way, gained dielectric functions put into Abelès formalism reference transmittance spectra can be calculated. A simpler way is to use a relation derived in Ref. [58], which we present here in a slightly different form:

$$\frac{\Delta T}{T_0} = C \cdot \frac{\Delta R(\alpha)}{R_0(\alpha)} \cdot \frac{\cos\alpha}{2(n_s+1)\sin^2\alpha}. \tag{6}$$

Here, T_0 is the transmittance of the bare substrate with refractive index n_s under normal incidence, ΔT is the difference between T_0 and the transmittance T with the layer in place. $R_0(\alpha)$ is the reflectance of the bare metallic substrate for the angle of incidence α and ΔR the reflectance difference. C is given by $C = \mathrm{Im}(\varepsilon(\omega))/\mathrm{Im}\left(-\frac{1}{\varepsilon(\omega)}\right)$ if the oscillators are weak [otherwise Eq. (6) cannot be used as the peak positions for $\mathrm{Im}(\varepsilon(\omega))$ and $\mathrm{Im}\left(-\frac{1}{\varepsilon(\omega)}\right)$ do no longer coincide]. As an approximation, C can be set constant in a narrow spectral range. For our PE model system and the range of the CH_2-stretching vibrations, we found that $C \approx 5$ is a valid approximation. In practice, the transmittance signals from the CH_2-stretching vibrations would be somewhat stronger than Eq. (6) predicts, due to a preferential orientation of the ODT molecules, which leads to slightly larger components of the transition moments parallel to the surface [55]. In fact, while in the literature, calculated values of the transmittance of ODT on Si (better characterized by SiO_2/Si where the thickness of the SiO_2 on the surface is in the range of a few nm) in the order of 10^{-3}% can be found,

experimental values for the transmittance signals of a monolayer of octadecylsiloxane (ODS) have been obtained, which are two orders of magnitude larger [62]. These experimental signals even exceed the signals of our model system PE for free-standing films. While the structure of ODS is closely related to ODT, its chain may have a slightly smaller inclination angle relative to the surface normal. Even together with setting $C=1$ in Eq. (6), this can, however, not explain a difference of two orders of magnitude between experimental and calculated values in literature.

Apart from dielectric or metallic substrates, sometimes, also the so-called buried metallic layer substrates (BML) are used. As the name suggests, these substrates consist of a metallic layer thick enough that it is virtually impenetrable to electromagnetic radiation at the spectral range of interest. Above this metal layer, a dielectric layer is placed. If the dielectric layer is comparably thin, i.e. 100 nm or below, the substrates show virtually the same behavior as without the dielectric layer [63]. For thicknesses around half a μm in the MIR (the exact thickness depends on the index of refraction of the dielectric), the properties change drastically. Even with normal incidence and without additional antenna, interference can lead to a fourfold signal enhancement [47]. Nevertheless, both types are called in literature BML-IRRAS, even if for the use of the BML substrates with the thicker dielectric layer interference-enhanced IR-spectroscopy (IEIRS) probably would be a better term in analogy to interference-enhanced Raman spectroscopy [64]. The strong advantage of BML substrates over conventional IRRAS substrates is that the signal of the analytes is not suppressed at or near normal incidence. In addition, at grazing incidence, the signal can be twice as high as that from conventional IRRAS substrates for the same condition [63]. The interference enhancement has a large bandwidth (comparably slow change of the enhancement factor with wavelength/wavenumber; this is obvious in Figure 4, right, where for PMMA both the signal due to the C=O vibration at 1732 cm^{-1} and the signal due to the CH_3 vibration at 2953 cm^{-1} are enhanced) and the absence of the Fano effect and of a plasmon band. For further details about thin-film IR spectroscopy, the interested reader is referred to Ref. [47].

In addition, to help in understanding the relevance of the choice of reference experiments, Figure 4 also gives some guidance on the extent molecules outside of hotspots can potentially contribute to the overall signal. As already stated, this is, in particular, relevant for analytes like PMMA, which cover the whole surface of a substrate. For these, a 30 nm-thick film can obviously already contribute considerably to the overall signal, depending on the used technique and the measurement conditions. The contributions might, however, be smaller than the one derived in Figure 4, as nanoantennas concentrate the impinging electromagnetic energy, which means that the interaction far from the antenna might be smaller than without an antenna. On the other hand, the enhanced near-fields have much larger extension than in the visible spectral range [65, 66].

When we start discussing these substrates in the following, we will, in particular, state enhancement factors if they are based on reflectance or transmittance measurements in relation to an analyte like ODT binding selectively in hotspots for the reasons given above. We will also give signal intensities so that they can be compared readily with those from reference measurements.

3 Top-down substrates

3.1 Particle-based substrates

The first substrate consisting of a periodic array of particles dates back to the year 2000 [67]. Jensen et al. used nanosphere lithography (NSL) to fabricate structures that resembled hexagonal bowtie structures, which had plasmonic bands at about 2930 cm^{-1} when the structures were fabricated on mica. The use of silicon and germanium as substrate material red shifted the plasmon bands to 1870 cm^{-1} and 1655 cm^{-1}, respectively. Accordingly, ATR crystals of these two elements were coated with the bowtie-like structures, and para-nitrobenzoic acid (PNBA) was used as the analyte. The results seem to show no advantages (i.e. in terms of significantly greater signal enhancement per unit area of metal) compared to metal island films. Accordingly, the overall signal was significantly lower, most probably due to the much smaller surface coverage of the bowtie structures compared to the metal island films. However, a definitive assessment is not possible, as only absorbance spectra were provided, which were comparably noisy due to a comparable low number of scans.

Three years later, in 2003, Crozier et al. systematically investigated a number of optical antenna array designs with different shapes ranging from linear to triangular and circular shape for the MIR, both theoretically as well as experimentally [68]. For the theoretical modeling of the dependence of the electric field strengths on the structures, FDTD was used, and the influences of antenna shape, length, and tip sharpness were systematically investigated. The results of these simulations were compared with far-field measurements. It was found that the antennas' resonance frequencies λ scale approximately with $\lambda/(2n)$, where n is the real part of the index of refraction

of the substrate material, independent of the antennas' shape. The FDTD simulations showed that the highest near-field intensity enhancements $|E|^2/|E_0|^2$ with factors up to 10^3 can be expected for triangular antennas with a tip angle of 0°, which is essentially a linear antenna. The reason for linear antennas having the highest enhancement is identified as the high surface charge density at the tips, i.e. the lightning rod effect. This means that the on-resonance effect is maximally enlarged by the off-resonance effect for linear antennas. The comparison between the modeled and measured extinction spectra of periodic arrays of the different antennas showed a good correspondence between both. Unfortunately, no SEIRS measurements were performed.

3.1.1 Linear nanoantennas

Linear nanoantennas have a number of different aliases in the literature. They are often also called "nanorod" antennas, "nanowires", or "nanobars". Actually, they can be regarded as having nanodimensions only concerning their height and width, both of which are usually equal to or below 100 nm. Because for SEIRS applications their resonance wavelengths typically lie in the range between 3 and 10 μm, their length l is approximately half of the resonance wavelength [69] (somewhat more precise is the equation $l \approx \lambda/(2n_{eff})$ where n_{eff} is the average real part of the index of refraction of substrate and ambient medium). Away from the optical frequencies, metals can be increasingly well considered as perfect electric conductors, which means that the properties of the antennas like the resonance frequencies depend less on the nature of the metal. While gold and silver are still the preferred metals, a number of other metals like Pt, Pd, Rh, Ru, Ir, Sn, Fe, In, Pb, and Pt–Fe alloys have already been in use in the early days of SEIRS [5]. In addition, Al, which gained in importance for SEIRS applications recently [70], has also been employed already, in particular also, for ordered arrays of linear nanoantennas. In 2001, Puscasu et al. investigated the spectral behavior of infrared frequency-selective surfaces of such arrays by simulations and experiment [71]. The authors varied the distances between the individual nanoantennas and their length and predicted the transmission of the substrates by comparably simple models. They also investigated "coupled dipoles", i.e. two nanoantennas within a unit cell having one short distance along the longitudinal axes (dimers). In a follow-up paper, they extended their investigations to coupled nanoantennas and examined also the spectral properties of arrays of crosses with regard to a potential application as infrared radiation sources [72].

About 6 years later, linear nanoantennas were for the first time used for SEIRS, in this particular case, however, not in the form of arrays, but as isolated particles [69] (as individual nanoparticles and arrays, where the individual unit cells have large-enough periods, show the same properties, we will also include the former in this review). Neubrech et al. used gold nanowires (cylinders) with a diameter of 100 nm and lengths between 1.2 and 1.7 microns the resonances of which were situated between 3200 and 2300 cm^{-1} (see Figure 5). According to the results of their experiments, a match between plasmon and molecular resonance optimizes the signal due to the latter. As an analyte, a monolayer of ODT was deposited onto the gold, and the transmittance of individual gold nanowires was measured using an infrared microscope coupled to a synchroton light source. This setup generated a signal in transmittance of 1.6% for the asymmetric CH_2 stretching vibration, which is comparable to the signal strength obtained by IRRAS measurements of ODT monolayers on gold.

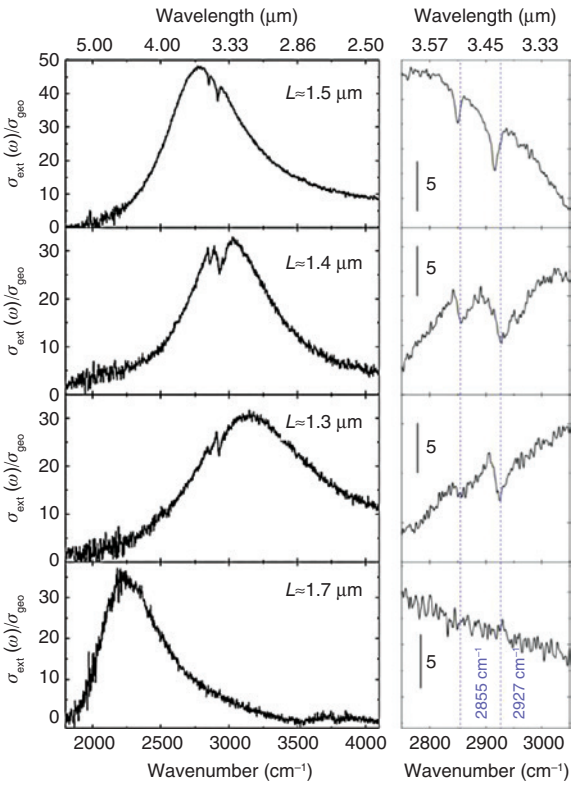

Figure 5: Experimental extinction cross-sections σ_{ext} (normalized to the geometrical cross-section σ_{geo}) for four ODT-coated wires with different L as indicated, and D = 100 nm on CaF_2. To the right, the zoom to the vibrational signals. Dotted lines: ODT vibration frequencies. Reprinted figure with permission from Ref. [69]. Copyright 2008 by the American Physical Society.

The authors relate the transmission signal from the system nanoantenna + analyte to that gained from an IRRAS experiment of an ODT monolayer at a high angle of incidence, which was converted into transmittance using Eq. (6) in combination with $C=1$. With the estimate that the signal of the antenna stems from approximately 150,000 molecules, an enhancement factor of the order of 10^5 results. For the near-field intensity enhancement around a nanoantenna, the authors found a maximum value of about 2×10^3 at the surface of the tip ends. Despite using a synchroton light source and accumulating 1000 scans per measurement, the spectra were comparably noisy but stem from a single nanoantenna in a circular area with a diameter of 8.3 μm. The signals show the typical Fano-like shape when the plasmon resonance was close to the molecular resonances and the typical dip structure as in Figure 1. Somewhat puzzling is the fact that for the accompanying modeling of the obtained spectra by means of the boundary element method, either a 100 nm-thick ODT layer or a higher dielectric background (a constant that accounts for the influence of transitions in the UV-Vis on the dielectric function in the infrared spectral range) had to be assumed for a good resemblance between simulation and experiment.

Stronger signal enhancement compared with isolated linear nanoantennas (or, equivalently, randomized arrays/arrays with periods larger than about 5 μm [73]) is possible if ordered arrays with optimized dimensions of the unit cells are employed. This was an important result of the work of Adato et al. [60]. In this work, the authors investigated first the far-field spectra of ordered arrays of linear nanoantennas with a length of 1.1 μm and periods of the unit cells, which were the same along and perpendicular to the long axes of the nanoantennas. Compared with random arrangements of the nanoantennas, the order leads to increased peak heights in the reflectance with, at the same time decreased full widths at half maximum and about a one order of magnitude increased near-field intensity $|E|^2/|E_0|^2$ of about 1600 according to FDTD simulations. As the nanoantennas were fabricated on Si, the high real part of the refraction index of the substrate shifted the bands in the range around 1650 cm^{-1}, therefore, being ideal for enhancing the amide bands of proteins. The authors used 2 nm-thick films of silk fibroin and obtained a signal strength $\Delta R/R_0=6.8\%$ of ordered arrays compared to 0.9% in the case of randomized structures for the amide I band at 1660 cm^{-1} with a very good signal-to-noise (S/N) ratio despite a comparably low number of scans. They found this increase in signal strength to be in agreement with the 10-fold increase in the near-field strength predicted by the FDTD simulations. The authors also investigated the signal from thicker films in order to examine the spatial extent of the near-field enhancement and seemed to find a saturation for 40 nm-thick films. However, their data can also be interpreted to allow for a spatial extent of up to 100 nm, which would be in better agreement with newer findings [65, 66]. This large near-field extent is a consequence of the fact that the evanescent fields of the plasmons are less strongly bound to the surface in the infrared compared to the visible spectral range.

Diffractively coupled nanoplasmonic arrays were also in the focus of Liberman et al. [74]. Usually, the array substrates are investigated by FTIR microspectroscopy, which means that the arrays are not illuminated approximately by plane waves traveling along the normal of the substrate, but by light focused by the microscope objective onto the substrate. Accordingly, the illumination cone consists in dependence of the numerical aperture (NA) of the objective, of a distribution of rays with different angles of incidence. According to the findings of the authors, already modest departures from normal incidence can lead to a significant performance decrease both in terms of the near-field enhancement as well as concerning the reflectance signal strength (a decrease of up to 20% was found), while the peak positions were only slightly affected. The authors suggest to slightly detune the corresponding arrays from the grating coupling conditions for normal incidence. The idea behind this detuning is to obtain substrates the characteristics of which are only moderately changed by the angular spread caused by the usual FTIR microscopy-employed Schwarzschild objectives. Unfortunately, SEIRS measurements were not part of this study. Therefore, the actual impact of the studied effect on SEIRS is hard to assess. The angular dependence of near- and far-field response of ordered linear nanoantennas was further investigated by Maß and Taubner [54]. They showed that by changing the angle of incidence, the plasmon resonance peak can be tuned by about 400 cm^{-1}. To obtain a shift as large as possible, it is of the advantage, according to the Bragg coupling condition, to use a substrate with a real part of the index of refraction as low as possible. Therefore, the authors chose CaF_2 as a substrate material. Experiments flanked by FDTD simulations showed that angle tuning allows to increase the signal by a factor of about 2. The overall maximum achievable transmittance signal was about 3% with a good S/N thanks to recording the spectra with at least 512 scans. This signal was achieved for the 2918 cm^{-1} CH_2-band of 16-mercaptohexadecanoic acid (16-MHDA), which has bands very comparable to the ones of ODT. This signal intensity is the highest achieved for antisymmetric CH_2-stretching vibrations

enhanced by linear nanoantennas so far. However, due to the fabrication process, it is possible that the antennas are on pedestals, which, as is discussed later in this section in detail, might provide an additional contribution to the overall enhancement. The authors also provide an interesting discussion on the dependence of enhancement factors from the choice of the reference measurement. By referencing to an IRRAS spectrum with p-polarization and large angle of incidence, they found a maximal enhancement factor of about 3700, which is of the same order as the near-field intensity enhancement calculated by the authors.

In a follow-up study of [74] from Liberman et al. [75], a slightly different group around the same first author investigated an approach to further optimize diffraction-coupled plasmonic arrays for SEIRS. A general problem in the search for optimized substrates is the impossibility to scan the complete parameter space by numerical methods. Instead, the authors propose to concentrate on the change of observable properties and suggest focusing on absorbance as the figure of merit (FOM). We disagree with the authors that absorbance is an observable quantity and think, as already detailed in Section 2.2, that absorbance (in contrast to "transmittance absorbance" or "reflectance absorbance") is a quantity that cannot be readily revealed with a conventional FTIR spectrometer. Nevertheless, the authors use reflectance absorbance and claim that silk fibroin films with a thickness of 50 nm on a bare and unstructured Au substrate cannot be successfully detected (based on the findings in IR thin-film spectroscopy summarized in Section 2.2, this might be the case for normal incidence on gold). The limited value of the reflectance absorbance reveals itself also by the fact that using it leads to partially negative absorbance values for the system chosen by the authors. After performing a background correction, a swarm optimization algorithm implemented in Lumerical (a commercially available FDTD program) was used to optimize the parameters of the substrate. Interestingly, while CaF_2 substrates lead to a 10-fold higher enhancement of the local fields compared to silicon, the optimal period for the unit cells is found to be about a factor of 3 larger on CaF_2, which means that the density of the nanoantennas on the substrate should be about an order of magnitude smaller. It seems logical to assume that both factors (higher enhancement of CaF_2 vs. lower density of nanoantennas) should cancel out each other; nevertheless, the silk fibroin seems to produce a threefold higher reflectance absorbance on CaF_2-based substrates. Unfortunately, experimental results were not provided, so that it is not possible to see if the latter substrates, indeed, have an advantage over silicon-based substrates in terms of the achievable transmittance/reflectance signal of the analyte (at least for bowtie antennas, it was experimentally shown that they generate a slightly higher signal in reflectance on CaF_2 substrates than on Si, which proves that in this system, the higher-field enhancement overcompensates the lower antenna density [76]).

Another way to increase signal strength is to couple linear nanoantennas via nanogaps along the long axis of the antennas [77]. In this case, the coupling of the nanoantennas is not taking place via diffractive, but through near-field coupling (diffractive coupling was prevented in this and the following examples by choosing the distance perpendicular to the long axis to be 5 μm). Accordingly, the distances along the long axes of the nanoantennas were drastically reduced down to 60 and 20 nm, and the transmittance far-field spectra were investigated using ODT as an analyte. The signal of the antisymmetric CH_2-stretching vibration of the ODT reaches about 1% in the case of the 20 nm gaps and roughly half of a percent in the case of the 60 nm gaps, with a comparably good S/N due to recording the spectra with at least 2000 scans. The actual reference measurement is not detailed, but a value for the enhancement factor is provided being 2×10^4. Based on this enhancement factor, there seems to be no advantage compared to the isolated nanowires presented in Ref. [69]. However, the plasmon resonance for the 60 nm gap structure was somewhat detuned, which was even more in the case for the 20 nm gap structure, so that a fair performance comparison between isolated nanowire and gap structure might not have been possible (disregarding the fact that the signal strength might not generally be maximum if plasmon and vibrational frequency coincide). The same authors further narrowed down the gaps via photochemical metal deposition. In Ref. [73], they report about a red shift of the plasmon of the gap structure between the particles of an array of four linear antennas in a row separated by small gaps with increasing exposure time, which is a consequence of the narrowing of the gap. Together with the red shift, the band height of the plasmon band decreases, which is a consequence of the stronger near-field coupling and the fact that, in some cases, the gap vanishes completely leading to a complete detuning of the resonance due the doubling of the lengths of the corresponding nanoantenna. Gap sizes of less than 10 nm could be reached (starting from 40 nm). SEM pictures revealed, however, that photochemical metal deposition took place not only in the gaps but also on the surface of the nanoantennas, which were covered with "rather big gold grains". The authors argue, however, that this should not influence the properties of the nanoantennas. The spectral properties of

nanogaps were further investigated on dimers [78], where the authors showed that it is possible to obtain gaps with a size of less than 4 nm. A careful evaluation of the SEIRS performance of the individual dimers with nanometer-sized gaps was subsequently provided in Ref. [79]. The authors investigated and established the relationship between the SEIRS signal and the gap size by experiment and simulations. To that end, the authors chose to use a 5 nm-thick layer of 4,40-bis (N-carbazolyl)-1,10-biphenyl (CBP) as a test analyte, which features nine modes in the range between 1230 and 1630 cm^{-1}. While CBP belongs to the group of analytes forming a continuous layer, the thickness of the layer assured a comparable small contribution to the transmittance spectrum, which was also cross-checked by the authors (the maximum signal of a 5 nm-thick analyte film on a bare substrate in transmittance was experimentally determined to be 0.4% at 1450 cm^{-1}). They compared a number of dimers, with gap sizes ranging between 3 nm and 50 nm. For dimers with smaller gap sizes, all nine modes were visible, while for larger dimers, only three modes were detectable. The plasmon resonance wavenumber of the dimer with 50 nm gap size seemed to be with about 1800 cm^{-1} strongly detuned, while the dimer with the smaller gap size had its maximum in the transmittance spectrum in the middle of the above-specified range of the molecular vibrations of CBP. The two strongest modes lead to dips with a signal strength of about 2% in transmittance for the strongest band at 1450 cm^{-1}. The spectra show a good S/N despite a comparably low number of scans. Overall, the authors conclude that about one order of magnitude of signal enhancement (a factor of 20 according to the experimentally determined enhancement factors) is gained by decreasing the gap size from 50 nm to 3 nm, which would be twice as much as what can be gained by optimizing the diffractive coupling of the ordered arrays. The signal enhancement factors correlate well with the near-field intensity enhancements calculated by FDTD simulations.

A synthesis of both approaches, i.e. varying the longitudinal distance between two linear nanoantennas to investigate the near-field coupling and changing the transversal distance to study diffractive coupling was undertaken in Ref. [41]. In particular, the difference to Ref. [60] is that in the latter, the transversal and the longitudinal separation distances were simultaneously changed and the period in both direction was the same, while in Ref. [41], the transversal and longitudinal distances were changed independently. One main result of the study is that in the longitudinal direction, the distance can be decreased and, by that, the antenna density can be increased, without altering the plasmon resonance substantially until the distance reaches a value of $\lambda_{res}/(4n_s)$, where λ_{res} is the wavelength of the plasmon resonance, and n_s is the real part of the index of refraction of the substrate. When the distance is further decreased, a red shift of the resonance results. For changes in the transversal direction, it is observed that the far-field response increases until the distance reaches a value, which equals λ_{res}/n_s. By further decreasing the distance, destructive interference results, and the far-field response becomes weaker and the plasmon band broader until it vanishes. Therefore, the density of the nanoantennas on the substrate cannot be increased over certain limits. As a result, the authors give the following limits: $0.5 \le \lambda_{res}/(2n_S \cdot dx) \le 2$ and $\lambda_{res}/(n_S \cdot dy)$ slightly bigger than one, where dx is the longitudinal distance, and dy is the transversal distance. It is important to realize that this puts a kind of upper limit on the attainable signal strength of a substrate. If we assume nanoantennas with a length of 1100 nm and 100 nm width with a plasmon resonance wavelength at 5.88 μm, this means that the area of a unit cell is given by $(1.1 + \lambda_{res}/(4n_S)) \times ((0.1 + \lambda_{res}/n_S) = 2.78\ \mu m^2$. This gives a maximum surface coverage of 4%. Even if we assume that dx approaches zero as suggested by the authors, the maximum surface coverage cannot be increased to be more than 5.5% (where it has to be taken into account that the resonance wavenumber then shifts, and the lengths of the antennas has to be adapted accordingly. This, however, does not alter our calculation as we have assumed that $dx = 0$). Considering that the maximum enhancement is then only available in the volume between the tips of the nanoantenna, the maximum signal intensity attainable by linear nanoantennas seems limited. Therefore, it can be concluded that the main strengths of SEIRS substrates with sculpted nanoantennas is, in contrast to that of conventional metal island substrates, to enhance signals from analytes that can be brought in a controlled way into the hotspots rather than the enhancement of the signals from thin, or, let alone, thick films. On the other hand, it must also be stated that the electromagnetic energy impinging on a substrate can only be concentrated and not enhanced. Therefore, while it might be possible to optimize the interaction between antenna and analyte and the redirection of the impinging energy, a mere increase in the nanoantenna density cannot arbitrarily enhance performance and would have a natural limit.

While electron beam lithography has proved its worth for fabricating nanostructures, its application would still be much too expensive and time consuming for mass production. One of the alternative is nanostencil lithography [80]. The authors used this technique to fabricate arrays of linear nanoantennas and applied these for antibody

assays and detection of immunologically important small proteins. A seeming disadvantage of this fabrication technique is that the prepared nanorods show gold nanoparticles clustered around the surface of the antennas. The authors demonstrate by FDTD simulations that these clustered nanoparticles lead to an extra enhancement of the near-field intensity by a factor of 10 compared to nanorods (maximum value around 10^4) from which the nanoparticles were removed by dry etch post-processing. Binding of a protein leads to a dip in the reflectance at the position of the amide I band of about 4%. The dip is enhanced by binding of a corresponding antigen to 5%. The spectra show, in general, a good S/N ratio despite a low number of scans. The calculated enhancement factor is on the order of 10^4, which seems to be on the low side, but the authors employ a fair type of reference measurement (IRRAS with an angle of incidence of 80°).

Another approach for the fast fabrication of arrays of linear nanoantennas is femtosecond direct laser writing lithography [81]. The authors were able to produce high-quality large-area substrates with this method. They fabricated arrays with different distances dx in the longitudinal and dy in the transversal direction and confirmed the findings of Weber et al. [41] using CBP layers with a thickness of 5 nm. By optimizing the length of the antennas and the distances, they were able to obtain a transmittance signal of somewhat more than 10% for the strongest band of CBP at 1504 cm^{-1} with a very good S/N despite of a very low number of scans. For this signal, the authors estimate the enhancement factor to be 14,000.

While smaller distances between the tips of nanoantennas classically lead to higher field enhancements, quantum mechanics must be taken into account when the distances become smaller than a few nanometers. Classically, there is a clearly defined interface (the surface of the nanoantennas) that separates media with different properties. Quantum mechanically, the electrons of a metal are not confined within the volume confined by the interfaces, but can spill-out. The related effects on SEIRS have been investigated in Ref. [82] by examining the spectral enhancement of the vibrational band of CO. The amount of cold-condensed CO, that is the thickness of the CO-layer, was carefully controlled. The result of this investigation was that the enhancement shows a maximum, not directly on the surface but between 1.0 and 1.5 nm away from the surface. While the authors investigated an array of antennas, distances between the antennas of 1 μm and 5 μm parallel and perpendicular to the long axis ensured that near-field and diffractive coupling was prevented.

Another approach to experimentally investigate and trace the near-field enhancement is offered by a scattering-type scanning near-field optical microscope [83]. Alonso-González et al. used the s-SNOM to examine the near fields around single and dimer linear nanoantennas by spatial mapping of the surface-enhanced light scattering. The authors found clear evidence that resonant scattering scales with the electric field strengths to the power of four and speculate that in addition to absorption, also scattering might play an important role in the case of SEIRS (which has been confirmed in the meantime, cf. Section 2.1.1).

In contrast to previous papers in this section, Neubrech et al. investigated the vibrational signature of an inorganic analyte, namely, an about 3 nm thin SiO_2 layer naturally grown on silicon [84]. Silica gives a strong phonon-polariton signal between about 1050 and 1300 cm^{-1}. The main oscillator is located at about 1070 cm^{-1}, which is at the same time the wavenumber of the so-called transversal optical (TO) phonon [85]. The corresponding dip of the 3 nm SiO_2 layer did not appear in proximity to the TO wavenumber, but instead, closer to the longitudinal optical (LO) phonon at about 1250 cm^{-1} in the range of the Fuchs-Kliewer surface phonon polariton. A large separation between TO and LO wavenumber is a consequence of a large oscillator strength, much larger than those that usually can be observed for organic substances. Nevertheless, the relative transmittance signal is with about 1% comparably weak, but with a comparably good S/N, thanks to recording the spectra with at least 5000 scans. The authors calculate an enhancement factor in the order of 10^3, connect the comparably weak signal strengths with the high real part of the index of refraction of the silicon substrate and comment that usually much higher signal strengths can be expected for substrates with lower indices of refraction.

Following an idea used for rings [86], which will be later discussed in more detail, Huck et al. suggested to put linear nanoantennas on a pedestal to further increase enhancement [87]. In fact, a pedestal decreases the interaction between substrate and antenna, which increases the plasmonic enhancement, in particular, if substrates with large dielectric constants are used. In addition, the use of pedestals allows a greater surface of the nanoantenna to be accessible for the analyte. A third advantage is that due to a lowering of the effective refractive index, the nanoantennas need to be longer to keep the same resonance wavelength, which means that the surface increases even more. Furthermore, the height of the pedestals was adjusted in a way that an additional enhancement resulted from constructive interference between the waves reflected from the antennas and from the surface of the silicon substrate. Overall, these effects add up to

a 10-fold increased integrated near-field intensity and a signal for the strongest ODT resonance of 2.4% in transmittance with a very good S/N, also due to a higher number of scans of 3000 per measurement. No signal enhancement factor was provided in this work.

Linear nanoantennas can also be used for both SEIRS and SERS, as the length and the width of the nanoantennas can be changed independently [88]. If, e.g. a width of 60 nm is chosen (using CaF_2 as substrate), then the antenna shows a plasmon resonance at about 640 nm when a polarization direction perpendicular to the long axis is selected. This can be exploited to enhance the Raman signal when the 633 nm laser line is employed. Using methylene blue as an analyte, D'Andrea et al. could show that they obtain a moderate SERS enhancement factor of about 5×10^2. The SEIRS signal intensities are in the normal range with up to about 1.5% in transmittance, but a very good S/Ns demonstrated (number of scans or accumulation time not provided). The calculated SEIRS enhancement factor is comparably high, but based on a ratio of transmittance absorbance and reflectance absorbance.

So far, we have dealt only with horizontally oriented linear nanoantennas. Arrays of vertically oriented linear nanoantennas can be fabricated in a controlled fashion by irradiating thin gold films with single laser pulses [89]. The main characteristic of these nanoantennas is that, in contrast to horizontally oriented nanoantennas, their resonances can only be excited with non-normal and p-polarized radiation, similar to the resonances of molecules on a gold film. The resonances have roughly a wavelength $\lambda \sim 4l$, where l is in this case both the height and the length of the nanoantenna, as they have monopole character and are accompanied by a mirror image in the metallic ground plane. While the nanoantennas fabricated by laser pulses have a spike-like shape, arrays of vertically oriented tubular nanoantennas can be fabricated by a combination of focused ion beam milling and secondary electron lithography [90]. Malerba et al. investigated and compared the performance of arrays of vertically oriented nanoantennas to that of arrays of common horizontal nanoantennas. They find "a much stronger plasmonic response, compared to that achievable with the use of 2D configurations, leading to higher energy harvesting properties and improved Q-factors", which seems to hold a promising alternative to the obviously not practicable way of increasing the surface coverage of horizontal nanoantennas to making the available electromagnetic energy more accessible. As reason for this superiority, the authors identify the monopolar electric field distribution, which increases the near-field enhancement and leads to a radial energy flow parallel to the substrate plane due to enhanced lateral light scattering. In terms of near-field enhancement, the standing nanoantennas generated a maximum near-field enhancement of 140 at 8.5 μm, which compares favorably to the near-field enhancement of 60 reached by a comparable horizontal nanoantenna. This near-field enhancement could be further increased by fabricating arrays of slanted nanorod dimers by extruding them from a silver baseplate. This essentially promotes the concept of nanogaps into the third dimension (cf. Figure 6) [91]. By coupling the resonances of two monopoles, two resonances result, an "antibonding" with the same charge at the end of the monopole and a "bonding" based on different charges. Of the two, in particular, the antisymmetric

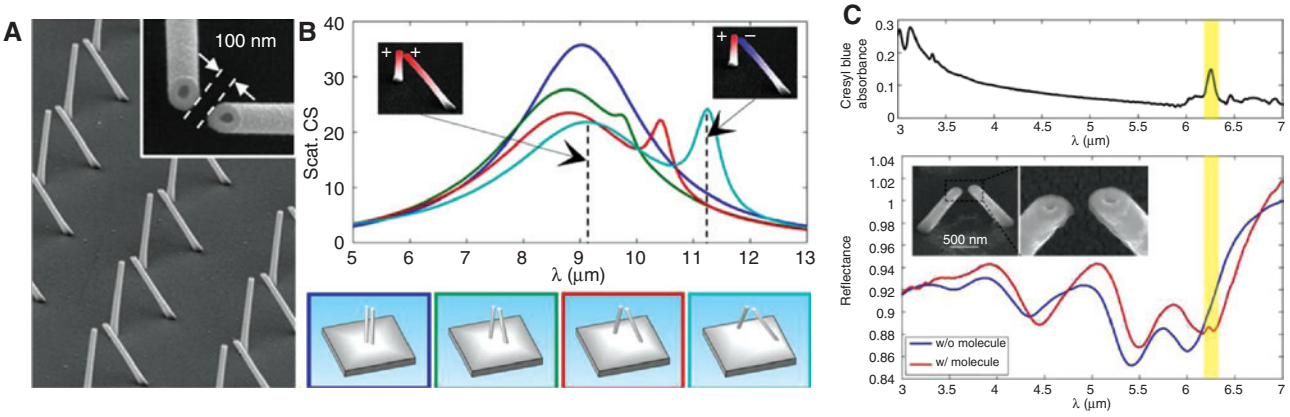

Figure 6: (A) Scanning electron microscopy (SEM) image of fabricated nanorod dimers. (B) Scattering cross-section spectra for different tilting angles α of the dimers. (C) Above: Measured IR spectrum of bulk BCB fluorophore. Below: FTIR reflectance spectra measured before (blue line) and after (red line) deposition of BCB on top of a nanorod dimer array (height 930 nm, $\alpha=32°$, $\beta=180°$, gap 100 nm, pitch 5 μm). The insets report SEM images of one dimer of the array after deposition. Adapted with permission from Ref. [91]. Copyright 2015 American Chemical Society.

bonding resonance shows a large near-field enhancement up to a value of 310. The authors managed to deposit an analyte, in this case brilliant cresyl blue (BCB), onto the silver layer and into the gap of the nanostructure. With a structure that has been tuned toward having the bonding resonance at 5.75 μm close to a resonance of BCB at about 6.3 μm, a signal of about 1% in reflectance resulted with a good S/N ratio (number of scans not provided).

Overall, these 3D structures show much promise, in particular, for sensing applications and SEIRS. A challenge, however, might be the need for a metallic ground plate, which could render targeted delivery and binding of analytes exclusively to the hotspots challenging.

At the end of this section, we shortly want to mention that linear nanoantenna arrays are the first SEIRS arrays that have been employed with regard to concrete biochemical applications. In particular, in aqueous solutions, in IR spectroscopy the water bands are quite strongly interfering with other bands of interest as they are extremely strong and in the region of the C-H stretching vibrations (O-H-stretching vibration) and of the amide bands (H-O-H bending vibrations). Therefore, path lengths larger than 10 μm are, even for high protein concentrations, not possible. Partly, this problem can be overcome by the use of attenuated total reflection spectroscopy. A superior approach seems to be to use linear nanoantennas, illuminate them from the backside, and gather the reflected signal. Adato and Altug used such a setup [92]. The Au nanoantennas were functionalized with a self-assembled monolayer of a biotin-labeled alkanethiol and spotted with streptavidin. Afterward, they were treated with anti-rabbit (goat host) ($^{(b)}\alpha$R(G)) IgG. In a third step, alternatively, anti-goat (mouse host) (αG(M)), rabbit IgG (R(s)) or mouse IgG (M(s)) were applied to bind either highly, weakly, or unspecifically to the $^{(b)}\alpha$R(G). All three steps could be clearly discriminated and, in the third step, highly, weakly, and unspecific binding could be distinguished. This could be achieved in spite of an also strong enhancement of the water-bending vibration, which provided a Fano-type interaction of a strength, which is comparable with the one between a bright and dark plasmonic mode.

A similar setup to the one used in Ref. [92] was employed by Limaj et al. [65] and used as "an infrared plasmonic biosensor for chemical-specific detection and monitoring of biomimetic lipid membranes". Instead of only one linear nanoantenna array for the detection of amide bands, an additional array with nanoantennas tuned for the CH_2-stretching vibrations was employed. This second array was used to detect the functionalization of an SiO_2 layer above the nanoantennas with the lipid membrane, while the first array allowed to examine the formation of a streptavidin layer above the lipid membrane.

A particular striking property of nanoantennas is that the plasmon and, therefore, the enhanced electric field, has a much larger spatial extension compared to enhanced fields due to plasmons in the Vis-NIR spectral range (this is a consequence of the lower skin depth of metals in the MIR spectral regions). Limaj et al. [65] investigated the spatial extension of the fields by increasing the thickness of a SiO_2 layer up to 100 nm. Even this far from the surface of the nanoantennas, an enhanced signal was clearly detectable, which agrees with the results gained 2 years earlier using layers of CBP [66] and with the results of FDTD simulations presented in Ref. [92]. Limaj et al. [65] see this as a clear advantage over SERS, which is somewhat in contradiction to some approaches presented later, where graphene and doped semiconductor structures are used to mimic the behavior of metals in the Vis-NIR regions to generate highly localized plasmons. As concluded in Ref. [66], in contrast to highly localized plasmons, which may be more useful for monolayers, the larger spatial extent of the plasmons in the MIR may be more suitable for thick objects like bacteria. On the other hand, for such applications, a clear disadvantage of this behavior was already discussed above, as the large spatial extension of the plasmons in the MIR leads to a small limiting value for the achievable density of the nanoantennas on the substrate, as the scattering from the antennas decreases the far-field signal and the near-field enhancement when the lateral distance becomes too small.

3.1.2 Gratings

Gratings were up to now comparably rarely used for SEIRS. One of the few works dealing with gratings is the paper of Wang et al. where the authors investigated gold strip gratings with regard to their enhancing properties [93]. The distance between the gold strip gratings [see Figure 7A)] was held constant at 1.6 μm, and the width was varied from 1.7 to 2.9 μm in steps of 0.2 μm for the investigation. Two different plasmon bands can be found in the MIR range, which belong to the plasmon excitations located at the edges, which touch the substrate (in this case CaF_2) and which are in free space/air. Using the grating coupling conditions, it can be shown that the band with the larger resonance wavelength originates from the edges in touch with the substrate. FDTD simulations of the gratings showed a maximum near-field intensity enhancement of about 300. The authors evaluate the performance of the grating using a "less than 30 nm-thick"

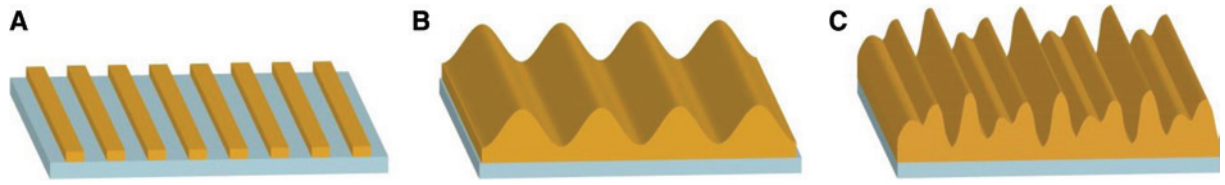

Figure 7: Various gratings used for SEIRS.

layer of PMMA and obtain a signal of up to 6% from the PMMA band at 1732 cm^{-1} with a good S/N despite a low number of scans. This signal is about 10 times larger than that which they obtain from an IRRAS measurement using probably the same measurement conditions. Based on an analysis of the latter measurement, the authors calculate the reflectance of a PMMA layer on a bare CaF_2 layer and use this as a reference measurement for calculating an enhancement factor. By taking into account the different number of "molecules" (monomer units?) in the spots, an enhancement factor of about 6000 results.

Even thicker PMMA films with thicknesses between 30 and 300 nm were used in the work of Petefish and Hillier to reveal the SEIRS characteristics of a grating fabricated by laser interference lithography [94] (see Figure 7B). As a result, these gratings, subsequently covered with silver, show a sinusoidal surface profile with a maximum height of 100 nm (3025 nm pitch) and 300 nm (1710 nm pitch). The first grating has a plasmon resonance around 1750 cm^{-1} the position of which can be slightly tuned by varying the angle of incidence, whereas the second grating has its plasmon resonance in the range between 3000 and 3300 cm^{-1} in dependence of the angle of incidence (55°–80°). The spectra of the PMMA-covered gratings are given in terms of reflectance absorbance. A recalculation shows that the signals of the CH_2-stretching vibrations amount to a reflectance signal of about 20% for p-polarized light with polarization direction perpendicular to the grating, while for the same polarization with the direction along the grating, about 5% is achieved. The enhancement for the C=O stretching vibrations is somewhat weaker, as a signal of 20% in reflectance is already achieved for the parallel orientation and a signal of about 25% for the perpendicular orientation.

The same authors investigated in a follow-up paper multipitched diffraction gratings (Figure 7C) [95]. The idea behind these types of gratings is to generate either multiple plasmons at different wavenumber ranges (larger differences in the pitches) or a broader resonance (small pitch differences). For the first alternative, the authors showed a proof of concept by generating a grating with simultaneous plasmon resonances at 3000, 4000 and 5000 cm^{-1}. This grating was not used in SEIRS experiments. For the second alternative, the authors introduced four different pitches and investigated three gratings with increasing pitch differences. When the difference is comparably small, the gain with regard to the width of the band is also comparably small. For larger differences, however, the individual plasmons manifest themselves in a fine structure that makes it somewhat hard to distinguish between this fine structure and molecular bands when analytes are present. To investigate the SEIRS performance, the authors used PMMA films with 262 and 715 nm thickness. Even though the authors focused on the comparably weak CH_2-stretching vibration features around 3000 cm^{-1}, these films are, in our opinion, too thick to allow a performance assessment, as already explained above.

Overall, we think that gratings are inferior compared to linear nanoantennas. Certainly, gratings are tunable by changing the angle of incidence. However, so are arrays of linear nanoantennas when the transversal distances are optimized. Linear antennas, however, can have a stronger enhancement than gratings due to the near-field interaction for small longitudinal gaps and due to the lightning rod effect.

3.1.3 Crosses

The first structure that we will discuss in this section is an individual antenna with a cross geometry consisting of four rods oriented at right angles [96] (see Figure 8B). Toward a gap at the central junction, the rods are tapered to exploit both the gap and the lightning rod effect to increase the enhancement. The antenna can be tuned by changing the length of the arms. Antennas with 575 nm long arms were found to have their plasmon resonance in the range of the CH_2-stretching vibrations of ODT and show a near-field intensity enhancement $|E|^2/|E_0|^2$ of about 2000. Experimentally, the individual nanoantennas gave a signal of about 0.07% in transmittance (recalculated from transmission absorbance) with comparably good S/N when covered by a monolayer. Antennas with 1200 nm-long arms gave a signal at 1662 cm^{-1} in the same order of magnitude for the amide I band when covered by a sub-monolayer of hemoglobin. A third sample with an arm length of 1800 nm

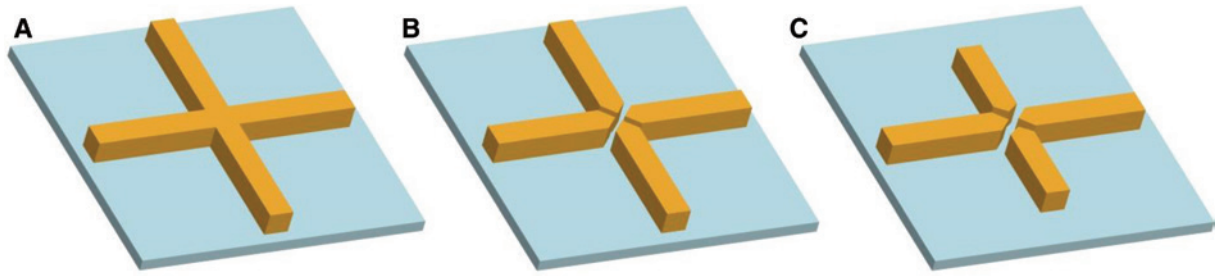

Figure 8: Various cross structures used for SEIRS.

was tuned for the 1070 cm^{-1} resonance of SiO_2. Here, the authors applied 50 nm-thick patches, which may be the reason that the signal did not appear in the Fuchs-Kliewer region as in Ref. [84] but at the TO position instead, as in ultrathin films, surface modes can be excited [63]. It is remarkable that the authors could use standard lab equipment to perform their experiments despite the comparably low signal intensity of individual antennas.

Generally, crosses as shown in Figure 8A are nothing else but two linear nanoantennas at right angles and, hence, without polarization dependence, and the crosses investigated in Ref. [96] are very comparable to dimers of linear nanoantennas [79]. It is, therefore, safe to assume that the performance could be increased further by exploiting coupling effects. In a follow-up paper, a subset of the authors of Ref. [96] investigated a similar structure, which is, however, made out of aluminum instead of gold, and only the two opposite antennas have the same length [70] (see Figure 8C). This allows to excite two different plasmons with which a large part of the infrared spectrum can be covered. The near-field enhancement factors $|E|/|E_0|$ obtained by FDTD calculations are somewhat lower if aluminum is used instead of gold due to higher ohmic losses. However, the formation of a thin Al_2O_3 layer of the surfaces allows a different surface chemistry to be exploited. Accordingly, the authors bind stearic acid to the surface (which has a backbone comparably to ODT) and find a signal of 0.3% in transmittance for the antisymmetric CH_2-stretching vibration with a good S/N despite a comparably low number of scans (100). Additionally, different types of binding of the acid group can be detected. Furthermore, the authors could make use of the 950-cm^{-1} phonon band of Al_2O_3 as internal standard.

3.1.4 Ellipsoidal particles

As already detailed in Section 3.1, according to Crozier et al. [68], linear nanoantennas show the highest enhancements of the electric field of all particles. Consequently, ellipsoidal-shaped nanoantennas should be inferior when used for SEIRS substrates if we disregard the fact that near-field enhancement is only one factor in SEIRS, albeit an important one. Laser interference lithography, a comparable cheap technique to fabricate cm^2-sized areas of nanoantennas, leads to exactly this shape [97]. Unfortunately, long and short axes of the particles as well as the pitch cannot be changed independent of each other when this fabrication method is used. Furthermore, two neighbored rows of antennas are moved by half a period relative to each other (hexagonal lattice, see Figure 9), which means that the axial distance is comparably large, and it is not possible to significantly enhance the near field by reducing the gap between two particles in the longitudinal direction. Correspondingly, FDTD simulations showed a maximum near-field intensity enhancement below 400. Particles with an aspect ratio of approximately 2:1 and with a resonance along the long axis at about 3000 cm^{-1} lead to a signal for the antisymmetric CH_2 vibration of ODT of about 1% in the uncorrected transmittance spectrum, which is a bit less than that of isolated linear nanoantennas. The baseline-corrected signal, however, shows a comparably strong Fano distortion and is nearly completely shaped like the real part of the refractive index at resonance. Furthermore, it is comparably noisy due to a comparably low number of scans. The authors calculate an enhancement factor of 67,000 by taking into account the number of molecules in the hotspot and ratioing the baseline-corrected signal to a transmittance signal of a monolayer ODT on gold (0.0087% for the asymmetric CH_2

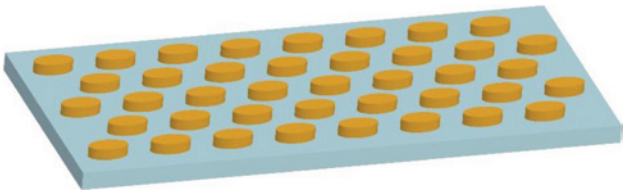

Figure 9: Substrate consisting of ellipsoidal particles in a hexagonal lattice.

vibration), which was calculated from IRRAS measurements using Eq. (6) with C = 1.

3.1.5 Bowties

The easiest way to fabricate bowties (Figure 10A) is the use of nanosphere lithography. As already detailed in Section 3.1, the first substrate, which dates back to the year 2000, consisting of a periodic array of particles was fabricated by this technique [67]. Thirteen years later, the idea of fabricating bowties by NSL was taken up by Hoffmann et al. [76]. The authors fabricated a larger variety of different substrates and showed that by varying the sphere size, they were able to cover the complete mid-infrared range of interest (cf. Figure 10B).

To evaluate the performance of their structures, the authors used PMMA layers with thicknesses between 35 and 41 nm and found signals of the C = O stretching vibration with a strength between 2.1% and 3.4% in reflectance with a good S/N. This is compared to an IRRAS signal of 0.45% of a 35 nm PMMA film on an unstructured gold substrate (the measurement conditions were not provided).

In a follow-up paper, Hoffman et al. used a two-step evaporation NSL with slightly inclined angles opposite to each other and relative to the evaporation source [98]. By that, two bowtie antennas, one above the other, resulted and were slightly displaced along the long axis of the antenna (see Figure 10C). The idea of the authors was to decrease the gap between the two triangular structures. The spectra of the substrate displayed two different but broad and overlapping modes, one excited with the polarization direction along the long axis at about 1150 cm^{-1} and the other at about 1450 cm^{-1}. The authors showed that they could obtain a good, albeit somewhat noisy, signal (up to 6.6% in reflectance) from the superficial SiO_2 layer of the silicon substrate, which showed up at the LO position at 1250 cm^{-1} and not in between the Fuchs-Kliewer region, which might indicate that either scattering [27] or surface modes dominate [63]. Using an appropriate three-oscillator model, the authors extracted the oscillator strength in dependence of the size of the gap and found that the absorption due to the SiO_2 mode first increased with decreasing gap extent but eventually decreased after running through a maximum at a gap size of 200 nm. This might be connected with an increasing number of bowties, which are, due to fabrication inaccuracy, connected, i.e. with closed gaps, which accordingly have drastically changed resonance conditions and are no longer able to enhance the analyte signal at 1150 cm^{-1}.

One drawback of all the antennas discussed so far, is that they typically work well in a usually very limited spectral range. This is a disadvantage that so-called log-periodic trapezoidal nanoantennas do not have as shown by Aouani et al. [99] (see Figure 10D). These nanoantennas can be seen as bowties with the long axis aligned vertically in the horizontal direction. Alternating on the left and right side, rectangles were removed so that a teeth structure remains. If light polarized along these teeth, i.e. perpendicular to the long axis, is incident on the structure, pairs of "induced horizontal dipoles are excited, which, in turn, induces a local vertical dipole between arms" of the bowties. As a result, four plasmon resonances appear in the corresponding spectra at 1410 cm^{-1}, 1910 cm^{-1}, 2400 cm^{-1} and 3150 cm^{-1}. The authors fabricated square arrays of approximately 150 nanoantennas with a pitch of 10 μm. The choice of this pitch "ensured that coupling between neighboring nanoantennas was insignificant, as confirmed by numerical simulations." The authors then bound carboxyl terminated alkanethiols (AT-EG6-COOH) to the structure, where the carboxylic groups were later converted to NHS ester. This latter compound has no bands between 1850 cm^{-1} and 2850 cm^{-1} like the large majority of compounds, but shows about 10 bands below 1850 cm^{-1} of which only two around 1100 cm^{-1} were visible. This somewhat impedes the main goal of the substrate, namely, to enhance the complete spectrum of a compound. Unfortunately, the authors only showed extinction cross-section spectra, albeit with a good

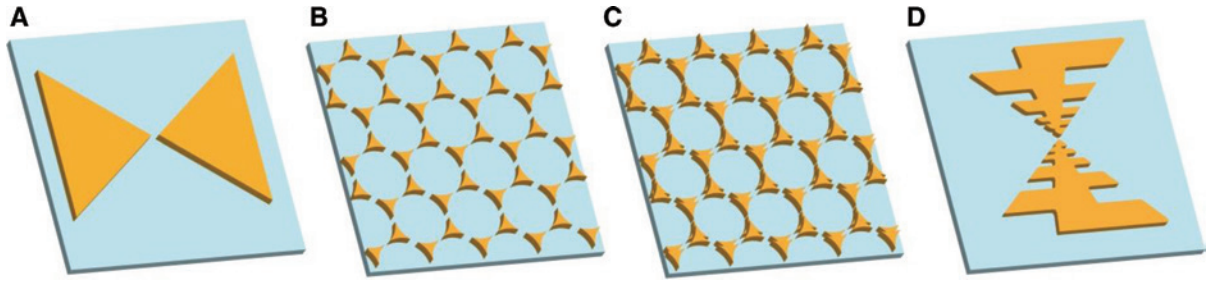

Figure 10: Various structures using bowties.

S/N, thanks to 1000 scans per measurement, so that the overall performance cannot be compared to that of other structures, but FDTD simulations show that in the central gap, electromagnetic field enhancements $|E|^2/|E_0|^2$ between 2 and 12×10^3 can be achieved.

3.1.6 Rings, split rings, crescents and dolmen-type structures

Nanocrescents (cf. Figure 11A) can be fabricated employing a technique called nanosphere-templated lithography (NTL), which is closely related to NSL, but uses an additional step, namely, argon ion milling, to remove metal that is not protected by the spheres. As the spheres cover only a few percent of the surface in a random fashion, the distance between individual spheres is usually comparably large, and interaction between the individual particles is not expected to occur. Bukasov and Shumaker-Parry used this technique to prepare nanocrescents, shortly after linear nanoantennas were introduced for SEIRS [100].

They measured transmittance and converted it to what they call "normalized extinction" (normalized extinction is based on $1-T$ instead of $-\lg T$). The authors showed that they could tune the plasmonic resonance of their nanocrescents using nanospheres of different diameters. They used ODT to show that overlap between plasmons and molecular vibrations leads to higher signal strength of the molecular bands. The strength of the transmittance signal in the comparably noisy spectra was not provided. However, the authors calculate a maximum enhancement factor of 46,000 by taking into account the area covered by molecules on the rings and ratioing the baseline-corrected signal to a transmittance signal of a monolayer of ODT (e.g. 0.004%), which was calculated from IRRAS measurements on silver using Eq. (6) with $C=1$.

In a follow-up paper, Cooper et al. could show that with even larger sphere templates, also larger nanocrescents could be fabricated from silver and gold, which have their plasmon resonance at even lower wavenumbers [101]. In addition, the authors showed that the excitation of plasmons of the crescents depends on the polarization of the incoming light. For example, nanocrescents made out of silver with a 2-μm diameter showed plasmon resonances at 2645 cm^{-1} and 1340 cm^{-1}, if the incoming light was polarized along the short and the long axis, respectively. Unfortunately, it seems that the resonance frequencies of the plasmons cannot be tuned independently. No SEIRS experiments were carried out, but FDTD simulations were undertaken, which show a maximum near-field intensity enhancement in the range of 10^3.

Split ring resonators (SRR, see Figure 11B) were first fabricated nearly at the same time as the crescents [102]. SRR arrays have an even more compact geometry than arrays of crescents in comparison with arrays of linear nanoantennas. Furthermore, they feature an internal nanogap, which additionally increases the near field. Made out of gold and with a radius of 170 nm, a width of 80 nm, and a gap of 30 nm, they feature a plasmon resonance around 2900 cm^{-1} when placed on a quartz substrate and illuminated with light polarized along the gap. After coverage with ODT, they show a transmittance signal of 1.9% of the band at 2918 cm^{-1}, which is similar in strength to that of ODT on linear nanoantennas. The authors estimate that the signal is generated only by about 22,000 molecules located in the gap, but they did not provide an enhancement factor. Numerical simulations demonstrated a maximum near-field enhancement below 85 in the gaps (cf. Figure 12). The spectra show a comparably good S/N taking into account that each spectrum consisted of 50 scans only. Coupling effects were not studied, but the SRR arrays had a comparably small period of 600 nm, and therefore, a much higher surface coverage could be achieved than the one for linear nanoantennas.

While in Ref. [102] electron beam lithography was used, Cataldo et al. [103] employed hole-mask colloidal nanolithography as a low-cost fabrication method. In contrast, this method does not lead to ordered arrays of SSRs but, instead, to a random distribution of the split rings due to the random distribution of the nanosphere templates, which, nevertheless, have their gaps all oriented in the same direction. The authors used both ODT as well as

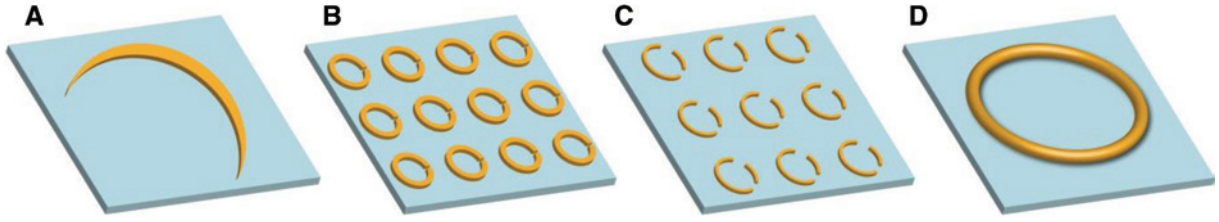

Figure 11: Various ring-shaped structures.

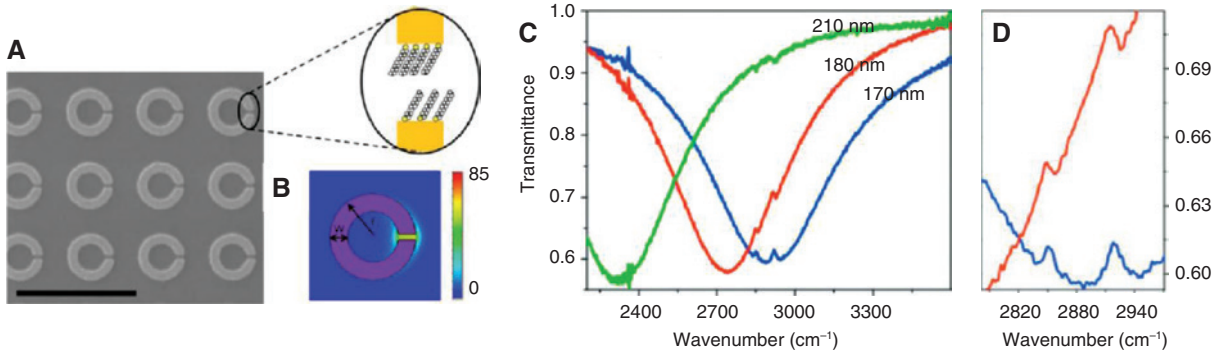

Figure 12: (A) Scanning electron micrograph of a typical SRR array. Scale bar is 1 μm. Inset shows a schematic of a SAM of ODT molecules in the gap of a single SRR for absorption spectroscopy. (B) Simulated near-field amplitude distribution around a SRR on resonance for polarization along the gap. (C) Measured transmittance spectra for three different SRR arrays with radii 170 nm (blue), 180 nm (red), and 210 nm (green) with the SAM. Two peaks corresponding to ODT absorption are clearly visible. (D) Close-up view of the resonance region in (C). Adapted from Ref. [102], with the permission of AIP Publishing.

completely deuterated ODT to show that their substrates have monolayer sensitivity. In both cases, the achievable signal was in the range of 1% reflectance for the antisymmetric CH_2-/CD_2-stretching vibration. The authors calculate an enhancement factor of 8000 by normalizing the area covered by molecules and ratioing the signal to a transmittance signal of a monolayer ODT on gold (e.g. 0.0039% for the antisymmetric CH_2-stretching vibration), which was calculated from IRRAS measurements using Eq. (6) with $C=1$.

Even somewhat earlier than the crescents and the SRR, the first arrays of asymmetric split ring resonators (A-SSR, Figure 7C) were fabricated [104]. These consist of rings with two gaps, which are asymmetrically arranged, so that one of the segments (arcs) is longer than the other. Made out of gold, they typically have a diameter of 1.2 μm and a width of 100 nm and have plasmon resonances in the range of 3–6 μm when placed on fused silica. The frequencies of the plasmon resonances depend on the individual length of the arcs and on the angular gap between them, which was varied between 10° and 50°. The authors tested the performance with PMMA films with a thickness ranging between 30 and 215 nm. For a 100 nm-thick film, the 5.8-μm PMMA feature showed a reflectance signal of roughly 15%. Other PMMA peaks, in particular, the CH-stretching vibration related bands between 3.27 and 3.33 μm, and the multiple bands in the fingerprint region between 6.66 and 8.33 μm could not be detected despite spectra with a comparably good S/N, thanks to a large spot size area.

While the authors originally speak of two individual peaks caused by the two arcs and a trapped mode in between, the spectra can better be interpreted as a bright-mode coupling with a dark mode leading to a plasmonic Fano resonance. In a follow-up paper, the resonances were investigated by resonance hybridization theory [105]. Additionally, the authors show simulations of the induced electric field, where at the two peaks a similar dipolar field distribution can be seen, whereas at the dip, a quadrupolar field distribution is exhibited.

In another follow-up paper, the authors investigated the hot spots and the dark mode by photothermal-induced resonance (PTIR) imaging [42]. In contrast to s-SNOM introduced earlier [83], “samples are placed on an optically transparent prism and illuminated with a tunable IR pulsed laser in a total internal reflection configuration to minimize direct light-tip interaction. The absorption of a laser pulse by the sample results in local heating, sample expansion, and mechanical excitation of the AFM cantilever in contact with the sample”. The authors further state, as one advantage of the method compared to s-SNOM, that “PTIR spectra are directly comparable with IR spectral libraries”. Here, one has to take into account that if spectral libraries contain absorbance spectra, then these were usually not measured directly but converted into absorbance using Eq. (3), in contrast to the PTIR spectra. The authors find that “at longer wavelength only the dark mode is excited wherein a larger fraction of the optical power is dissipated by the longer arc. At shorter wavelengths, a small admixture of the bright mode increases the power dissipated by the short arc and suppresses the power dissipated by the long arc via constructive and destructive interference.” The authors compared the spectra of PMMA-coated A-SSRs (thickness of the PMMA layer: 200 nm) taken at the hotspots and far away from the rings and find near-field enhancement factors of about 28. These much lower near-field enhancement factors, compared

to values of 10^2–10^3 as found for other nanoantennas with the help of numerical methods, result from the fact that the PTIR method has a lateral resolution of about 100 nm and, therefore, averages over the corresponding area. Furthermore, the comparable large thickness of the PMMA has to be taken into account.

The PTIR method was further applied to the A-SSRs in [106], wherein the authors investigated near-field asymmetries resulting from a non-zero angle of incidence and the use of polarized light. They found by FEM calculations that constructive interference between electric and magnetic dipolar excitations of the dark-mode can occur for non-zero angles of incidence that is turned into destructive interference when the path of the light is reverted. The authors confirmed their findings by PTIR measurements. Constructive interference is realized when light is falling in through the dielectric substrate from the short arc side and the light polarization is parallel to the sample plane and the long direction of the arcs.

This incidence scheme was also used to show that the employment of a metal-insulator-metal structure instead of a pure metal structure is able to increase the near fields by about 50% [107]. The authors realized this structure by fabricating A-SSRs consisting of $Ag/Ag_2O/Ag$ layers and compared their performance to A-SSRs consisting solely of Ag.

Finally, PTIR measurements were also used to investigate the influence of the period on the performance of A-SSRs [108]. For isolated particles, the authors found that A-SSRs show clearly the highest enhancements followed by c- and u-shaped rings, which showed about half of the enhancement of the A-SSRs with light advantages for the c-shaped rings, and, finally, by crescents with little more than a fourth of the A-SSRs' enhancement.

Furthermore, for all four types of investigated shapes, for an optimal far-field response, a larger packing density usually overcompensates any degradation due to destructive interference when the interparticle distances are decreased (however, the case $p \approx \lambda/n_{\mathrm{eff}}$, where p is the pitch, which was studied, e.g. for linear nanoantennas in Ref. [60] and which gives particularly strong enhancement by constructive interference, was not studied in Ref. [108]), in contrast to the near-field response, which is the strongest for the isolated particle.

Structures similar to the split rings can also be used to build a tunable SEIRS substrate [109]. To that end, Pryce et al. used different arrays of mostly u-shaped structures. For example, a u-shaped structure with a bar on top (SRR-bar, Figure 13A), two u-shaped structures with the openings vis-à-vis (Figure 13B) and different side lengths (like asymmetric split rings) and two u-shaped structures, also with the openings vis-à-vis, but with different base lengths and telescoped (Figure 13C). Furthermore, there is a dolmen-type structure with a gap between bar and metal stripes (Figure 13D). All of these structures have in common that the distance between the u-shaped structures or between u-shaped structure/metal stripes and bar on top can be varied by stretching the substrate, which consisted of polydimethylsiloxane (PDMS). This change in distance allows the resonance frequencies to be tuned.

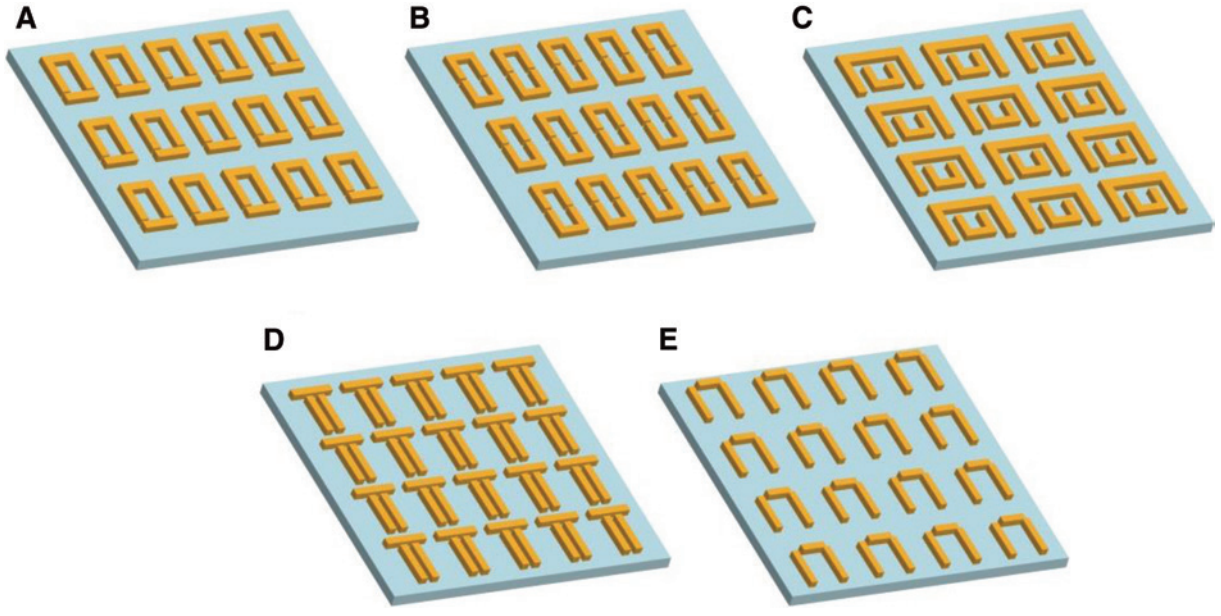

Figure 13: Various angular ring-shaped structures and Dolmen-type structures.

The authors show that the C-H-stretching vibration can be enhanced if one of the plasmon resonances is tuned toward the frequency of the C-H-stretching vibration. The authors find a signal enhancement factor, which is not area or volume normalized, of up to 180 compared to that of the bare PDMS substrate, which has a thickness of 1 μm, in terms of reflectance. The corresponding calculated maximum near-field intensity enhancement amounts to about 500.

Arrays of SSR-bars were further investigated in Ref. [110]. The authors showed that with increasing distance of the bar, the plasmon resonance gets blue shifted when light polarized along the bar is used. The performance was further tested using a monolayer of p-mercaptoaniline (pMA). For the minimal distance (40 nm), the strongest band of pMA at 6.31 μm showed a signal of 4.5% in reflectance, which decreased to 0.9% when stretched PDMS was used as a substrate. The spectra were mostly noise-free in spite of a comparably low number of scans (64). The authors also calculate signal enhancement factors using the reflectance of neat pMA as reference and taking into account the number of molecules in the hotspots, which are with 10^4 of the same order as the calculated maximum near-field enhancements.

Arrays of dolmen-type structures were investigated in Ref. [111] (Figure 13E). Their spectrum also showed a Fano-type plasmon resonance, but in contrast to the structure in Ref. [109], the distance between the two metal stripes was larger, and the bar was attached to one of the stripes. The authors used the structure because of the high-quality factor (i.e. the small linewidth) of the dark mode. As a higher near-field enhancement is achieved with the polarization direction along the metal stripes, reflectance spectra with and without a sample were obtained with this polarization. From these nearly noise-free measurements obtained by 256 co-added scans, the authors could derive the height of a protein A/G monolayer and that of a bilayer consisting of the protein and the IgG antibodies bound to it. Probably, as the peaks of the proteins were not directly visible in the reflectance spectra, the authors used first-frequency-derivative spectra to obtain the spectral signature of the proteins.

SiO_2 was already the subject of several SEIRS studies as detailed above [84, 96, 98]. In Ref. [84] Neubrech et al. found a dip comparably far away from the TO wavenumber (1070 cm^{-1}) and closer to the longitudinal optical (LO) phonon at about 1250 cm^{-1}, in the range of the Fuchs-Kliewer surface phonon polariton, while in Ref. [96], the signal appeared at the TO and in Ref. [98] at the LO position. The reason for this behavior might be the different coupling of the phonon to the plasmon mode. Shelton et al. [112] used differently sized split ring resonators to tune the plasmon resonance from 6.6 μm to 13.8 μm and showed that there exists a strong coupling between both modes, which could be well explained by a coupled oscillator model. This model predicts a repulsion of both modes and an energy gap explaining the transparency window between them. The lower-energy mode becomes phonon-like at the TO frequency for higher plasmon frequencies, whereas the higher-energy mode becomes phonon-like around the LO frequencies for lower plasmon frequencies. Huck et al. showed for materials of cubic symmetry that scattering from gold nanoantennas lead to bands at the LO positions even under normal incidence [113]. None of the findings have, however, been discussed taking into account the occurrence of surface modes in ultrathin films [63]. In addition, in the case of glassy SiO_2, there is a very controversial discussion about the occurrence of bands at the LO positions even in bulk form and in the absence of scattering and under normal incidence [114, 115]. The existence of a medium order in the glasses, in general, suggests that amorphous materials, and in particular vitreous SiO_2, have optical properties different from crystals of cubic symmetry, but similar to randomly oriented polycrystalline materials with small crystallites in which mixed TO-LO modes are allowed even under normal incidence [116]. This complicates the separation of the influences from SEIRS scattering, surface modes, and the mixed TO-LO modes for this material.

Finally, arrays of closed rings were investigated in Ref. [86] as SEIRS substrates (Figure 7D). Compared to the other structures presented in this section, they do not show any polarization dependence, something which the authors see as a particular advantage, as the beam provided by the spectrometer needs not to be weakened by a polarizer. The authors compared conventional rings and rings on a pedestal and found that the latter have a tripled signal in reflectance, which amounts to about 3% for the amide I band in practically noise-free spectra thanks to 256 co-added scans per measurement. By FDTD simulations, the authors calculated a maximum near-field intensity enhancement of about 350 for the rings on a pedestal compared to about 250 for the conventional rings. The overall advantage of rings on a pedestal compared to conventional rings is caused by a larger sensing surface and better accessible near fields, thanks to the pedestals. The authors see this as a general finding transferable to other kinds of nanoantennas. As mentioned above, this has been demonstrated in the meantime also for linear nanoantennas [87].

3.2 Hole-based substrates

Based on Babinet's principle, the plasmonic properties of hole-based substrates can be easily understood. Following this principle, the reflectance spectrum of a particle-based substrate should resemble the transmittance spectrum of the corresponding inverse structure and vice versa if the polarization direction is rotated by 90° (cf. Figure 14) [117]. Despite the fact that hole-based substrates have a number of advantages compared to particle-based substrates, and their use started already in 2003, they did not get the attention they deserve, and so far, only a few works deal with their use for SEIRS.

3.2.1 Square holes

The first use of hole-based substrates for SEIRS dates back, as already mentioned, to the year 2003 [118]. Williams et al. used commercially available Ni microarrays consisting of square holes (Figure 15A), which were not especially adapted to the task, e.g. by tuning their

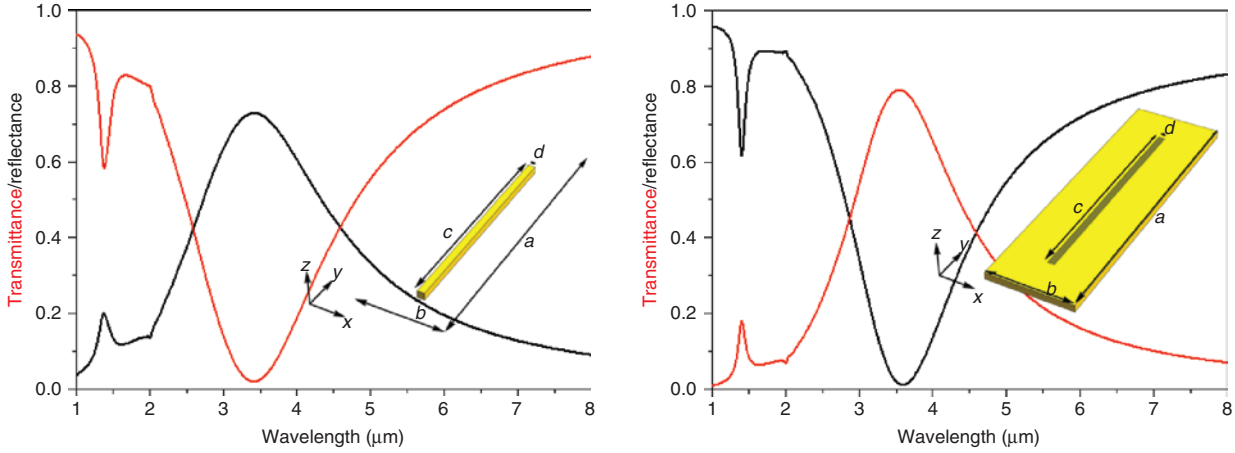

Figure 14: Comparison of the reflectance and transmittance spectra of an array of linear nanoantennas in free space with that of the inverse structure (an array of slits). For the nanoantennas, the polarization direction is parallel to the long axis, whereas for the slits, it is perpendicular to the slit.

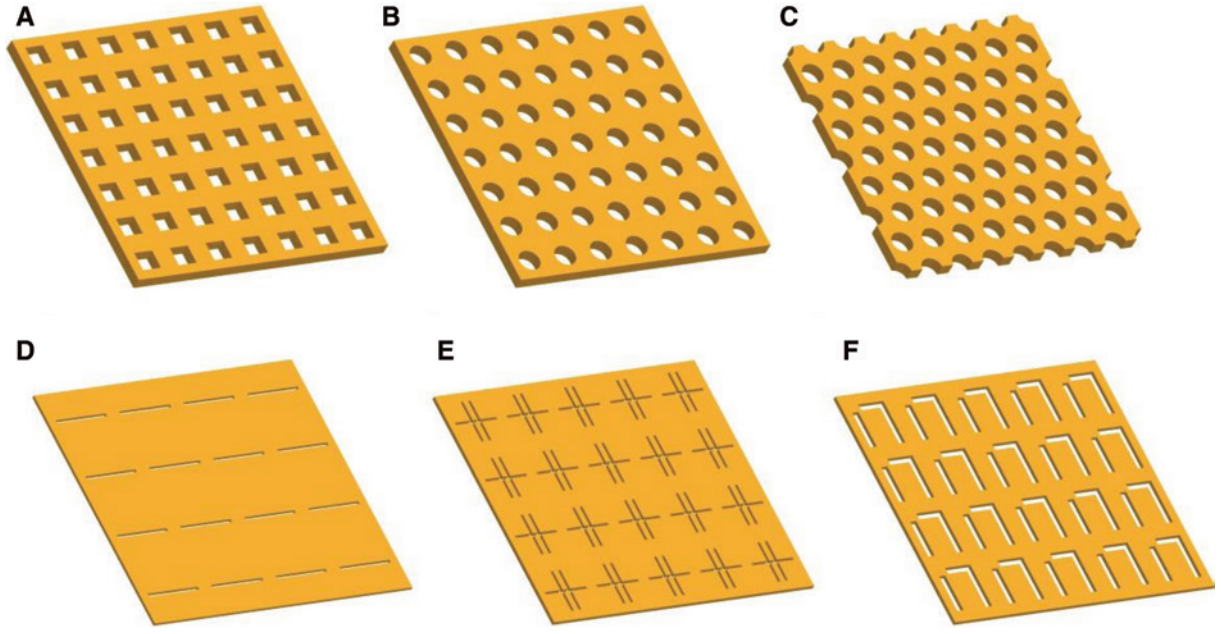

Figure 15: Various hole-based substrates.

plasmon resonances, to enhance the IR absorption of ODT. The size of the square holes was $6.5 \times 6.5\ \mu m^2$, and with a pitch of 12.5 μm, the holes occupied a little more than 25% of the surface area. Nevertheless, they showed a plasmon-supported transmission maximum of about 80% at 700 cm^{-1}. The effect of showing a higher transmittance than the relative surface area the holes occupy is called extraordinary optical transmission [119]. The authors report a 100-fold signal enhancement compared to IRRAS experiments. Unfortunately, only the absorbance spectra of the substrate with adsorbed ODT were provided [converted from transmittance with the help of Eq. (3)], which had a good S/N despite a comparably low number of 25 scans averaged.

In a follow-up paper, the authors reported about a way to tune the Ni-meshes, namely, by coating them electrochemically with copper [120]. The reduction of the hole size resulted in a narrowing of the resonances due to a surface plasmon lifetime increase. The substrate was used to study the catalytic reaction of methanol to formaldehyde after oxidation of the copper surface. The authors present transmittance spectra, but due to the complicated nature of the plasmonic background, peaks due to the molecular vibrations are hard to discern. It seems that the strong C-O-vibration, which peaks at 1028 cm^{-1} and dominates the methanol spectrum, gives rise to a transmittance signal of about 1% in comparably noisy spectra (each the average of 40 scans). The same copper-coated Ni meshes were used to further study the SEIRS spectra of several alkanethiol monolayers with chain lengths from 8 to 18 carbon atoms [121]. In the CH_2-stretching vibration region of the spectra, transmittance signals of about 0.5% can be seen (cf. also Figure 3 in Ref. [122]). Nevertheless, the signal enhancement was strong enough to detect the much weaker CH_2-wagging and rocking modes and their progression with increasing chain length, thanks to a good S/N achieved by averaging 1000 scans.

The same group of authors employed the same substrate to investigate nanoscale assemblies within the channels to control the flow of light in these channels [123]. In addition, the authors examined the interaction of the largest transmission resonance of the substrate with the rocking vibration of hexadecane molecules at 721 cm^{-1} in a micrometer-thick film on the mesh by tuning the plasmon resonance frequency through varying the thickness of the film [124].

Much finer meshes of aluminum with square hole sizes between 0.53 and 0.76 μm as well as smaller pitches between 1.37 and 2.00 μm were used by Limaj et al. [125]. These meshes showed plasmon-assisted extraordinary optical transmission peaks at higher wavenumbers due to the smaller sizes. In particular, using a hole size of 0.53 μm and a pitch of 1.37 μm, a transmittance maximum at 2966 cm^{-1} results. The drawback of the smaller sizes is that even then the transmittance is lower than 0.013, and the spectra show comparably much noise despite averaging 512 scans. Using a triple lipid layer as an analyte (a Langmuir-Blodgett film together with liposomes), these layers caused a relative transmittance signal of about 3%, which was still clearly above the noise level. Also, the authors could determine the thicknesses of the layer. Overall, however, metallic meshes with square holes do also not seem to have the potential to compete with conventional metal island films.

3.2.2 Circular holes

In 2012, 9 years after the first use of square hole-based substrates for SEIRS, the first substrates based on circular holes appeared [126] [see Figure 15B)]. Nishijima et al. fabricated and studied these substrates with periods between 2.9 to 3.9 μm and hole diameters, which amounted to half of the period. Their spectra showed the same trend as those of the square hole substrates, namely, a blue shift of the transmittance maxima with decreasing period and hole diameter. In the maximas, the transmittance amounted to between 7% and 15%. To test the performance of the substrates, the authors used azobenzene films of unknown thicknesses and compared the results with those of azobenzene films on a silver metal island film with a nominal metal thickness of 10 nm. Unfortunately, the Ag deposition rate, on which the metal island size and, therefore, the SEIRS performance of the silver island films depends, was not given, and the spectra were processed to absorbance so that a comparison of the performance with that of other substrates cannot be made. The authors also calculated the maximum near-field intensity enhancement of their substrates and found 43 as the maximum value for the mode around 1000 cm^{-1}.

In a follow-up paper, the hole-based substrate was slightly modified to be used in SF_6 gas sensing [127]. Instead of square lattices, the authors switched to hexagonal ones (see Figure 15C) due to better transmission properties. Employing a lattice constant of 3.3 μm and a diameter of 1.65 μm of the circular holes in a 100 nm-thick silver film on silicon, a transmittance of about 40% between 900 and 1000 cm^{-1} was reached. The gas cell consisted of two of these substrates at the beginning and the end with the silver-coated side oriented inward. The authors provided plots of the absorbance $A = -\log(I/I_0)$ over the concentration, where I is the detected signal and

I_0 the signal without SF_6, using the asymmetric stretching mode of SF_6 at 943 cm^{-1}. In our opinion, the resulting graphs do not show a linear relationship in contrast to what was assumed by the authors. With regard to performance, a 27-fold absorbance enhancement was reached compared to the case where the structured silver layers were oriented outward. The authors also calculated the near-field intensity enhancement of their substrates using FDTD simulations and found a maximum value of 16000.

3.2.3 Slits

While linear nanoantennas have been studied for some time, the inverse structure given by slits was not investigated until recently, i.e. until 2015 [128]. Huck et al. made a systematic study of nanoslits (see Figure 15D) and compared their properties with those of linear nanoantennas. Accordingly, for a polarization direction perpendicular to the slit, strong plasmon resonances are excited around 3000 cm^{-1} for a slit length of about 1 µm as could be expected from Babinet's principle. A strong advantage of slits compared to nanoantennas is that the integrated near-field intensity increases nearly linearly with the distance from the surface within the slit, in contrast to nanoantennas, where the near fields decrease much stronger with distance. Concerning the maximum near-field intensity enhancement, both the array of nanoantennas as well as an array of slits with the same resonance wavenumber showed a maximum value of 2500. Accordingly, the authors find a practically noise-free (due to at least 1000 co-added scans) reflectance signal of about 6% for the asymmetric CH_2-stretching vibration, which is about three times higher than that for the corresponding nanoantenna arrays, despite an area-normalized enhancement factor of 13,500, which is only about a sixth of that of a reference nanoantenna (93,400; the reference measurement was an IRRAS measurement that "was corrected since the IRRAS geometry already provides an enhancement due to the mirror-dipole effect and the grazing incidence of light", cf. Figure 16). The authors also investigated the influence of slit width and the periods of the arrays and found that, in particular, the slit width has a strong influence and is optimal at 50 nm.

One year earlier, in 2014, Cetin et al. published a study about the properties of essentially H-shaped slits where the slit connecting the two parallel and vertically oriented slits was extended beyond the vertical slits [129] (see Figure 10E). This system showed highly anisotropic plasmon resonances, one polarized along the horizontal slit and two in the vertical polarization direction. Based on FDTD simulations, the authors showed that a particular strong near-field intensity enhancement $|E|^2/|E_0|^2$ of up to 3×10^4 can be gained for this latter polarization direction and the mode with the higher wavelength. This mode was tuned to have the same wavenumber as the amide I and II bands of proteins, and the same protein bilayer system as in Ref. [86] (nanorings on a pedestal) was used. For the slits, the authors found an about three times stronger response compared to the nanorings on a pedestal with a completely noise-free signal, thanks to 256 co-added scans, of about 10% in transmittance. The minimum slit width investigated in this study was 100 nm, and it seems

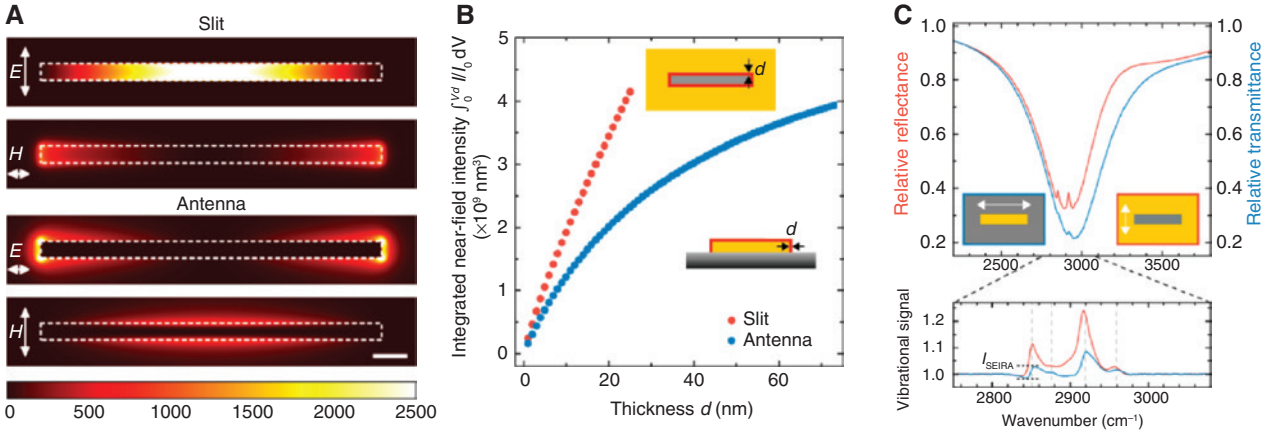

Figure 16: (A) Near-field intensity distribution of a resonantly excited nanoantenna array as well as a nanoslit array in a plane parallel to the substrate at half height of the nanoslit/nanoantenna (scale bar: 100 nm). (B) Near-field intensity integrated over a shell volume surrounding the nanostructure (see inset) with increasing thickness d. (C) Relative IR reflectance (transmittance) of a nanoslit (nanoantenna) array covered with a monolayer of ODT. The dimensions of both arrays are $w = 50$ nm, $\Delta x = \Delta y = 1.7$ µm and $L_{Slit} = 1000$ nm ($L_{Antenna} = 1050$ nm). The lower panel shows the baseline-corrected vibrational signal of the ODT molecule. Adapted with permission from Ref. [128]. Copyright 2015 American Chemical Society.

safe to assume that the response could be even further increased by decreasing the slit width.

Also in 2015, Cheng, Yang, and Gao published a study about a dolmen-type slit structure [130], which is the inverse of the structure investigated in Ref. [111]. Accordingly, the structure consists of two parallel-oriented slits with one slit ending on top in a horizontal bar-shaped slit, so that it looks like an inverted L (see Figure 10F). The maximum near-field intensity enhancement is according to FEM simulations in the range 10^3–10^4. Like its inverse counterpart, the structure shows a strong internal Fano resonance in the virtually noise-free spectra (512 scans co-added). The authors used PMMA films to investigate the SEIRS performance. For a 12.8 nm-thick film, a signal strength of 9% in reflectance results for the C=O stretching vibration of the PMMA. Probably influenced from the internal plasmon Fano resonance, the molecular signal is also extremely strong Fano-shaped and distorted. Using a reference measurement of the reflectance from PMMA on a bare gold substrate (signal strengths of the C=O stretching vibration ≈0.007, which is comparably strong for a near-normal incidence measurement), normalizing to the number of molecules and correcting for the mirror-dipole effect and the screening effect, the author determines an enhancement factor of approximately 163,000. Overall, it seems that slits are due to the electric field distribution within the slits extremely advantageous and superior to antennas, in general.

3.3 Perfect absorbers

Perfect absorbers (PAs) are metamaterials (i.e. periodic nanostructures with unit cells of dimensions that are much smaller than the wavelength of light at which they operate, so that the structures are smaller than the resolution limit, and effective optical constants result; being strict, however, this condition is usually only approximately fulfilled) with at least one resonance with unity (or near unity) absorption. This means, due to $A+R+T=1$, that reflectance and transmittance are effectively zero at the resonance. The first perfect absorber structures consisted of a dielectric layer sandwiched between an electric resonator structure (a double split ring resonator) and a cut wire and was designed for the microwave spectral range [131]. In the optical spectral ranges, the usual design is a continuous layer of a metal thick enough to account for $T=0$, on which a dielectric spacer layer is deposited [132]. On top of this dielectric layer, another metallic layer is placed, which is structured and consists either of particles or holes (see Figure 17). The resonance frequency of the metamaterial is both a function of the thickness of the dielectric layer and the particle dimensions (or lateral distance between holes). Both are tuned in a way that the impedance of the metamaterial matches that of free space with the consequence that $R=0$. This is achievable, as the structures have both an electric dipole resonance due to the particle or hole and a magnetic resonance due to antiparallel currents in the particle and the metallic ground plane. As a consequence of this impedance, matching comparably sharp resonances (high-quality factors) with strongly enhanced near fields results. A further property worth mentioning is the fact that the bands due to the fundamental mode of PAs only marginally change with the angle of incidence. Therefore, the use of a microscope objective does not substantially alter the spectrum in contrast to antennas on a dielectric substrate. All these advantages seem to render the PA as a perfect SEIRS substrate. However, for particle-based PAs, it is important to emphasize that PAs rely on critical coupling ($\gamma_{Ae}=\gamma_{A0}$). Therefore, counterintuitively, molecular analytes should show the weakest signals when the frequency of the molecular vibration and the plasmon are matched (cf. Figure 1, medium and Ref. [26]), if the oscillator strength is weak and scattering does not play a role. For medium strength vibrations like the C=O stretching vibration, this is usually not a problem except if manufacturing deviations lead to the case where $\gamma_{Ae}-\gamma_{A0}\approx\gamma_P$.

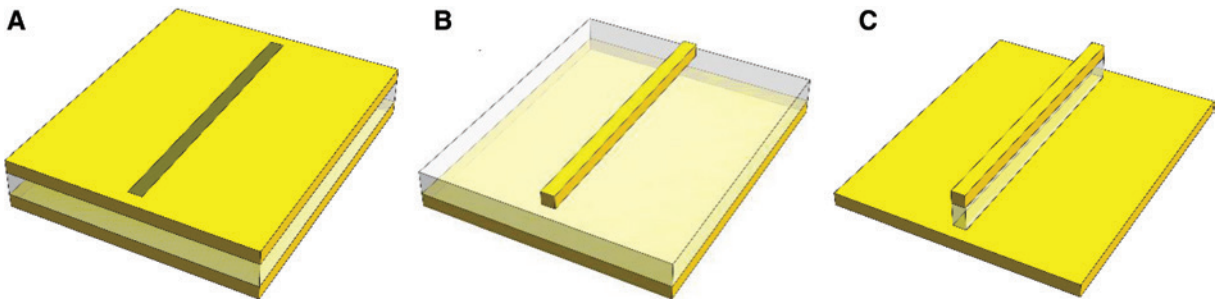

Figure 17: Principle perfect absorber designs.

3.3.1 Metal-insulator-metal structures

The first PA structure tuned for the infrared spectral range seems to be that proposed by Liu et al. [132]. This structure consisted of an array of gold crosses on a 185 nm-thick layer of Al_2O_3 and a gold ground plane with a resonance wavelength at about 6 µm. The first PA structure that was actually investigated with regard to its SEIRS performance employed also crosses as particles, however, with a broken symmetry. As a result, they showed two distinct resonances for the polarization direction along the remaining mirror symmetry element as a result of the two different arm lengths [133], as the bar between them acts as a wire reflector (see Figure 18A). With this design, the authors achieved for both resonances an absorption of more than 98% despite possible separations of more than 1000 cm^{-1}. The authors also investigated the nanoparticle analog and found that the near-field intensity enhancement factors $|E|^2/|E_0|^2$ for the PA design were with a maximum value of about 5000 equal for both resonances, in contrast to those of the nanoparticle analog, and between about two- and sixfold higher. To test the performance, the authors selected the parameters of the PA in a way that one resonance was located around 2850 cm^{-1} and the second around 1750 cm^{-1} after coating with a 4 nm PMMA film, aiming at the C-H and the C=O-stretching vibrations at the same time. The spectra showed a good S/N (number of scans not detailed). The C=O vibration gave a reflectance signal of about 10%, while the C-H vibrations were barely visible and below 2%, which we relate to the weak oscillator strength in connection with the critical coupling condition (the C-H vibration signals are generally much weaker for PMMA compared to ODT; the fact that the corresponding plasmon resonance was slightly detuned both with regard to frequency, and critical coupling condition might have helped, cf. Figure 19).

Four years later, in 2016, the same principal idea was realized, but instead of asymmetric crosses, two metal stripes of different lengths were used as particle(s) [134] (see Figure 18B). Again, the two occurring plasmon resonances were tuned for the C-H and the C=O stretching vibrations of PMMA. The resulting signals were about two times stronger, which is a consequence of the PMMA layer employed in the later study being thicker (10 nm compared to 4 nm in the earlier study). The spectra were virtually noise-free and the result of 256 co-added scans.

Another cross structure, however, symmetric and in a hexagonal lattice, was investigated by Li et al. [135]. The arrays of gold crosses on Al_2O_3 and gold showed two absorptions, the fundamental mode between 6 and 7 µm and a higher-order mode at around 2.5 µm. The SEIRS performance of the PA was checked with films of Parylene C, "tens of nanometers in thickness". The spectra show all bands of the Parylene C, but due to the unknown thickness, a performance evaluation is not possible. The authors calculated the near-field enhancement intensities of their structures with the help of FDTD simulations and found maximum values between 10^4 and 10^5.

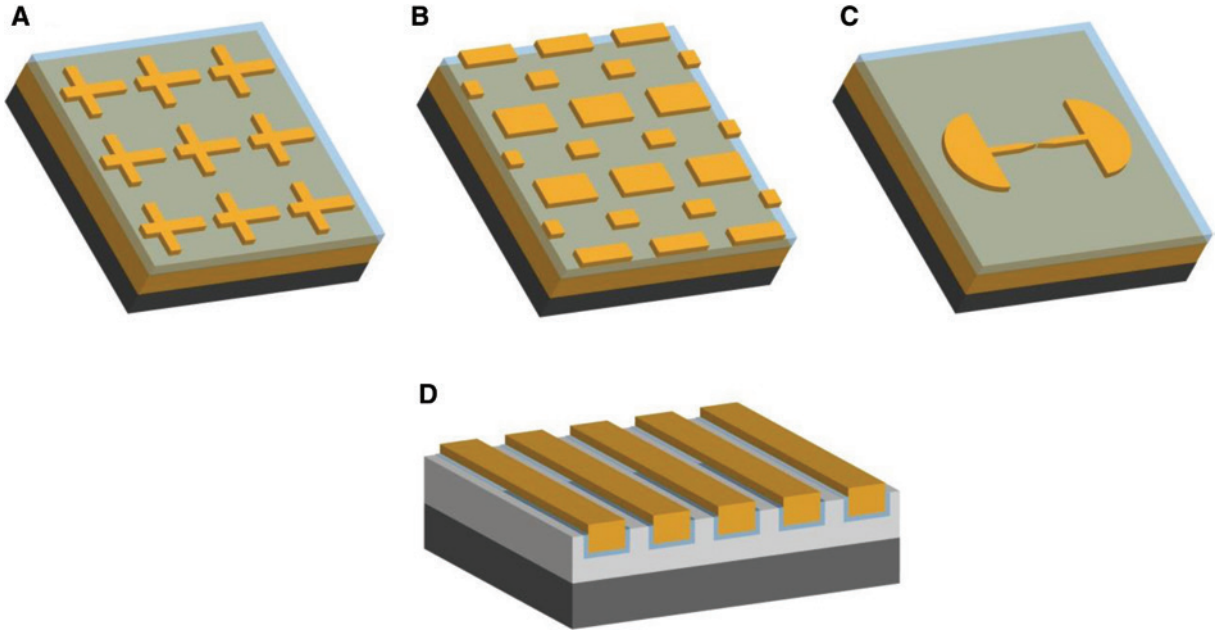

Figure 18: Various perfect absorber designs used for SEIRS.

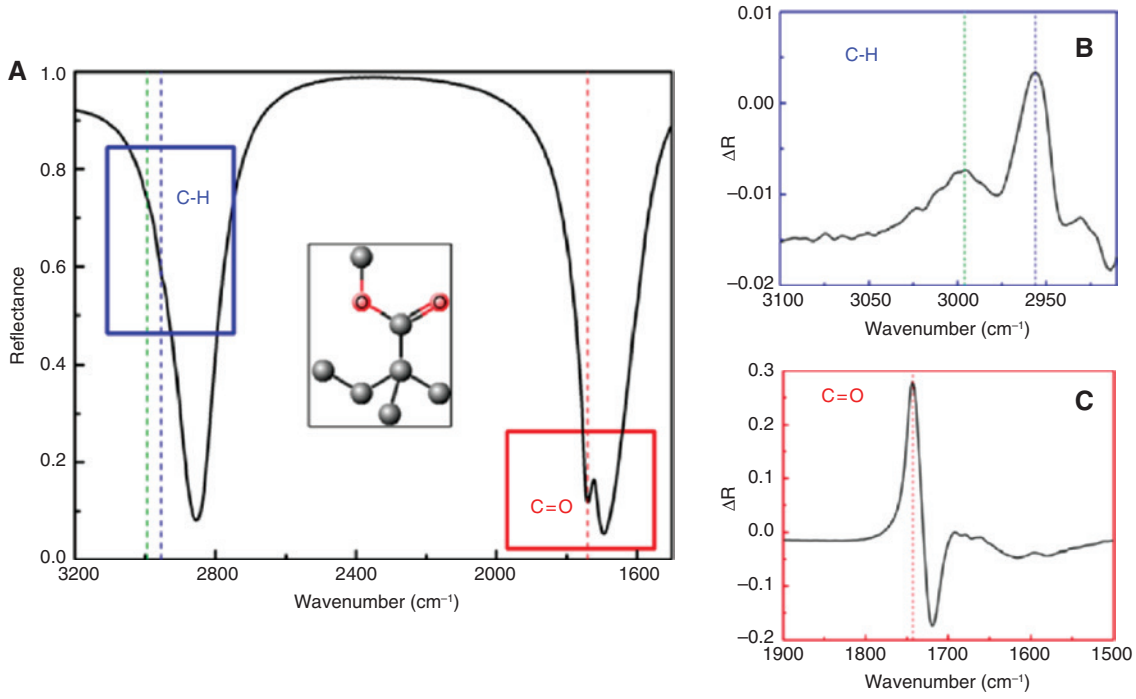

Figure 19: SEIRA spectroscopy of PMMA on the absorber. (A) Reflectance spectrum of the absorber after the coating of a 4 nm-thick PMMA film. Characteristic vibrational stretches of C=O and C-H are visible on the spectrum as indicated by the dashed lines. The inset shows the repeat unit of PMMA polymer. (B) Reflectance difference spectrum of the C-H group and (C) C=O band. Reprinted with permission from Ref. [133]. Copyright 2012 American Chemical Society.

An alternative shape of the nanoantennas, namely, disks, was employed to design the PAs for SEIRS in Ref. [136]. Chen et al. used the layer stack $Al/Al_2O_3/Al$ and nanosphere lithography to structure the Al top layer to spheres with a hexagonal lattice. The disk diameter was controlled by the O_2 plasma etching time. The disks with diameters between 1.8 and 2.2 µm lead to plasmon resonances between 1700 and 1500 cm^{-1}, respectively. They showed a maximum near-field intensity enhancement calculated by FDTD simulations of about 1000. The authors functionalized the Al_2O_3 surfaces with 10-carboxydecylphosphonic acid (10-CDPA), and C=O vibration bands appeared in the corresponding reflectance spectra (only reflectance absorbance spectra with a medium S/N were provided). This functionalization opens up the way to investigate biomolecules like proteins, etc.

A similar design, also relying on disk-shaped particles, but made out of gold and on top of a Ta_2O_3/gold layer system and with a cubic lattice, was employed in Ref. [137]. The authors showed that by varying the diameter of the disk, the plasmon resonance can be tuned from about 2600 cm^{-1} to 6000 cm^{-1} while keeping the period of the lattice constant (in this work, the structures were not optimized with regard to perfect absorption). Dodecanethiol (DDT), which has bands very comparable to those of ODT, was used as an analyte to investigate the SEIRS performance. The authors find that they obtain already comparably strong signals if the molecular and the plasmon resonance is detuned by about 200–500 cm^{-1}, with the advantage that the signals are nearly free of Fano distortions, which conforms to the systems shown in Figure 1 (Section 2.1.1). Unfortunately, the authors show only absorbance spectra, so that the performance cannot be properly evaluated. However, the presented baseline-corrected spectra of DDT seemed to be completely noise-free and, therefore, of very good quality (300 scans co-added). The authors provided an enhancement factor normalized to the number of molecules, but unfortunately based on absorbance given by 2.2×10^6.

As in the work introduced before, Brown et al. relied on a metal/insulator/metal (MIM) structure that was not tuned toward perfect absorption [56]. Instead, the fan-shaped gold nanoantennas on top of a SiO_2/gold layer system (Figure 18C) were tweaked for maximum enhancement relying on interference. The authors compared different related systems like dimers of rods and circles as well as bowtie antennas and found the highest near-field intensity enhancements $|E|^2/|E_0|^2$ for the dimers of fan-shaped antennas with up to 1.2×10^5. In addition, they determined the additional near-field intensity enhancement through

the interference effect introduced by the metallic mirror to be a factor of about 5, which is somewhat more than intuitively expected. With regard to performance, a 3×3 array is able to provide enough spectral contrast to raise ODT signals well above the noise level with standard lab equipment, on the expense, however, of taking an average of 125 spectra each with 100 scans (note that the distance between antennas was large enough to avoid collective effects). Generally, the concept behind the fan-shaped antenna seems to be directed more toward single molecule sensitivity and not in the direction of perfecting overall substrate performance. Evaluation of the latter, however, is not possible due to the use of reflectance absorbance spectra.

The opposite way, namely, not to optimize the thickness of the dielectric layer to obtain interference enhancement, but to decrease the thickness of the dielectric layer in an MIM structure as far as possible to obtain gap enhancement, is pursued by Chen et al. [138]. The structures consist of gold stripe gratings on Si, which are coated by a thin layer (3–5 nm) of Al_2O_3 and, subsequently, by silver. Before usage, the structures are template stripped, and the Al_2O_3, which builds a u-shaped nanocavity (Figure 18D), is partly removed to expose this cavity to the analyte. The plasmon resonances are caused by Fabry-Perot interferences, and their frequencies can be tuned by the width of the strips (again, no original PA design). According to FEM simulations, the (Al_2O_3-filled) gaps showed a near-field intensity enhancement of 1600. The small gaps are entered by the analyte, in this case, benzenethiol. Background removal seems to be complicated due to the Fabry-Perot interferences and was not performed. Only reflectance absorbance spectra were shown, which are comparably noisy. The authors also used graded nanogap structures as broadband resonator based on varying the metal stripe widths, but, again, comparably noisy spectra resulted.

Another grating-based metamaterial absorber was introduced in Ref. [139], consisting of gold/MgF_2 stripes on a gold layer. In contrast to the other designs presented so far, it was not the fundamental resonance that was tuned to a molecular vibration but the first overtone, which needs non-normal incidence to be activated. The idea of the authors was not to maximize the near-field enhancement, but to minimize the background signals using the overtone "to gain a large S/N ratio for better sensitivity". The latter goal is achieved, and the reflectance signal of the asymmetric CH_2 vibration of a 16-mercaptohexadecanoic acid monolayer amounts to about 0.5%.

A last approach introduced in this section will be the combination of perfect absorption with extraordinary optical transmission proposed in Ref. [140] (see Figure 17A). In contrast to the other metamaterial (perfect) absorber, it is not based on particles but on arrays of slits in the first two layers of a SiO_2/gold/Al_2O_3/gold layer system. Both gold layers are with 50 nm thick enough that in the infrared spectral range, virtually no light is transmitted. Accordingly, to reach perfect absorption, at the plasmon resonance frequency, all light that is incident on the whole surface must pass through the slit. Therefore, the electric field is strongly enhanced within the slit. The top SiO_2 layer has the function to prevent the analyte (ODT) from binding at any other location then to the gold surfaces within the slits. By concentrating analyte and fields within the slits, a filled slit should generate a signal for the asymmetric CH_2-stretching vibration of ODT as large as 25% according to FDTD calculations. In practice, the signal is even larger, in spite of the slits being only partially filled. The authors show, also by FDTD calculations, that decreasing the slit width from 50 to 10 nm, even with detuning the plasmon resonance to the spectral region between hydrogen stretching vibration and fingerprint region, the whole infrared spectral region of interest could be enhanced without causing appreciable Fano-like distortions (see Figure 20). Overall, this is no surprise, as these findings are in full agreement with those presented in Section 2.1.1 and Figure 1 with the help of the temporal coupled-mode theory. Accordingly, the signal of the analyte is already notably enhanced comparably far off resonance (cf. also [137]). Indeed, decreasing the slit width could be seen as a very successful concept taken over directly from metal island films. Those, however, could not be described by a single plasmon oscillator in contrast to the slits, which might be able to explain the existence of stronger Fano-like distortions in these systems. Once such small slits are technologically within reach, such a system could generate analyte signals with intensities in the range of conventional metal island films.

3.3.2 Structured metal perfect absorbers

Recently, several papers showed that impedance matching and perfect absorption is possible with all-metal structures. From those, we selected two structures that were designed for working in the infrared spectral range and might show some promise for SEIRS. The first structure consists of an array of 3D u-shaped structures, where the tines are oriented perpendicular to the surface [141] (Figure 21A). Two of these u-shaped structures share the center of the bar (the second u is linked to the first u by a 90° rotation around a rotation axis perpendicular to the

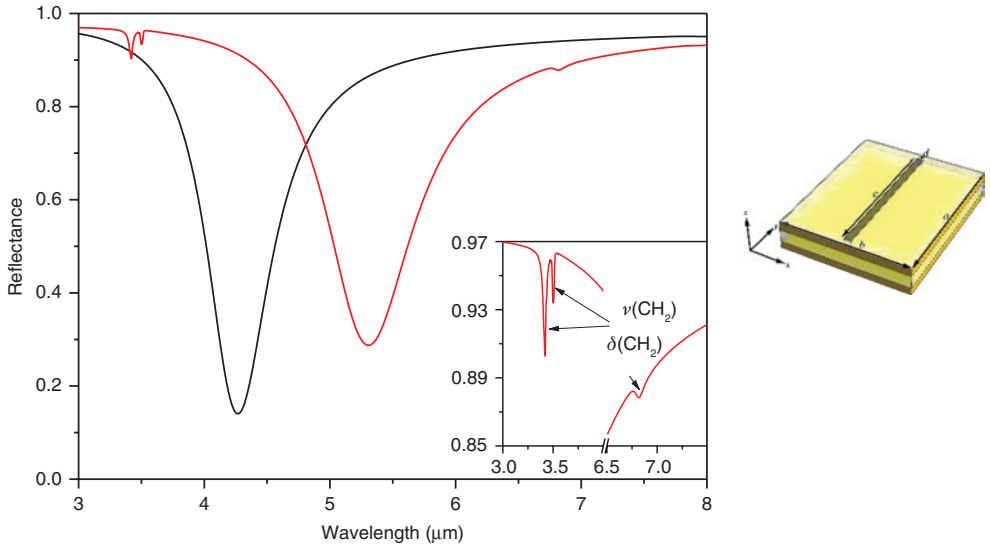

Figure 20: Simulated reflectance spectra of a slit perfect absorber for normal incidence. Compared are the *x*-polarized spectra of the slit PA with empty slit (black) and slit filled with PE (red). The inset gives an enlargement of the regions with PE absorptions.

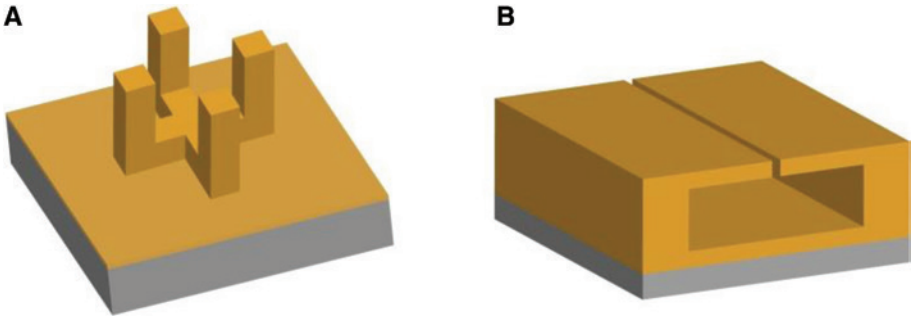

Figure 21: Two all-metal perfect absorber designs.

surface through the center of the bar), and these combined structures build arrays with a period of 4 μm. The height of the bar and the tines are, e.g. 0.6 and 1.6 μm, respectively, and their width is 0.3 μm. The two cross-standing u structures were fabricated by a two-photon polymerization process and were covered afterward by a 35 nm-thick gold layer. Depending on the height of the tines, the spectral region between 1000 and 2000 cm^{-1} was covered, and up to 90% absorption was reached experimentally. Unfortunately, the field intensity enhancement was not provided.

The second structure, a so-called electromagnetic Helmholtz antenna consists of a buried slit-box resonator, which is infinite along the slit axis and has a squared shape with height = width = 480 nm made out of gold [142] (Figure 21B). On the surface, only the slits are visible, which constitute a one-dimensional array with a period of 3 μm. The slit width and height are 2 and 30 nm, respectively. According to simulations, the field shows an electric field intensity enhancement of 10^6 at a wavelength of 15 μm within the slits. While this would be very interesting, it is not possible to fabricate these structures with the tools available now and, probably, for some time to come.

3.4 Non-metal-based approaches

It is typical for metals that, while they are characterized by an individual plasma frequency that provides an upper frequency limit for the existence of plasmons, they tend to approach perfect conductors toward the microwave and radiofrequency spectral ranges. Intimately connected to this property is that the confinement of surface plasmons decreases from several nanometers in the Vis-NIR spectral range to up to about a hundred nanometers in the mid-infrared spectral range. While this can be beneficial if the structures to be investigated have about the same extension, it may be of advantage for monolayer sensing if the extent of the interaction is mostly limited to this monolayer. Also,

while in the Vis-NIR spectral ranges, individual metal particles show less interaction, and the packing density can be high, the larger extensions of plasmons in the infrared can be a disadvantage, as they cause negative interferences and decrease the packing density. A solution to this problem is to use materials that support plasmons but have lower plasmon frequencies than metals, ideally somewhat beyond the high wavenumber limit of the MIR. Those materials can be certainly doped semiconductors as well as graphene.

3.4.1 Graphene

Graphene does not only support plasmons at frequencies lower than twice its Fermi energy level E_F, but additionally allows tuning the E_F by applying electrostatic fields. Its usefulness in relation to infrared plasmon sensing was theoretically investigated by Vasic et al. [143]. In particular, the authors investigated a nanoribbon structure of graphene on SiO_2 and the change of its properties with a variation of the distance between the ribbons, the width of which were kept constant. In addition to the tuneability, the authors investigated the accessible figures of merits for refractive index sensing of thin monolayers of analytes (thickness = 1 nm), the spectral response in dependence of film thickness and the SEIRS properties. The authors found by calculation that a reflectance signal of more than 5% should be possible if a maximum imaginary dielectric permittivity of 3 at the molecular resonance was assumed. For the assumed thickness of 1 nm, this would be an enormous signal, but the simulation does not take into account that the strongest imaginary dielectric permittivity for an organic material in the infrared spectral range (caused by the C = O stretching vibration) is not higher than about 1.5 [94]. For proteins, it seems that the corresponding vibrations that involve the C = O stretching vibrations (amide I and II) are even weaker and do not show values above 1 [144]. It is, therefore, hardly surprising that even with an 8 nm-thick protein bilayer consisting of recombinant protein A/G and goat anti-mouse immunoglobulin G (IgG), a maximum signal of about 1% in transmittance was achievable, albeit with a good S/N (cf. Figure 22) [144]. For the experimental realization, the authors used a nanoribbon structure of graphene with a width of 30 nm and a period of 80 nm in which the ribbons were connected at both ends (Figure 23A) to allow tuning them by applying a bias voltage. Using values between –130 and –20 V, the plasmon could be tuned from 1800 to about 1300 cm^{-1}, which is a remarkable tuning range.

A similar nanoribbon structure of graphene on SiO_2 was used for IR sensing of perylene-3,4,9,10-tetracarboxylic dianhydride (PTCDA) monolayers and acetone and hexane in the gaseous state [145]. In this work, the authors did not apply a bias voltage to tune the plasmon of the graphene but used adsorption and desorption of NO_2 instead. The signal strength of the C = C and C = O stretching vibrations of the comparably thin layers of PTCDA (0.6 nm) amounted to a signal of about 0.25% in transmittance with a mediocre S/N. Even if these results are overall not on par with those obtainable by optimized metal structures, the potential of graphene-based solutions has not yet been fully exploited. In this regard, it is worth mentioning that a completely spectrometer-free approach was recently suggested, which "instead simply involves infrared lamps and electrical doping of the graphene structure through an externally applied gate voltage" [146], which might pave the way to very cost-effective SEIRS applications.

3.4.2 Semiconductors

The first use of structures made out of doped semiconductors for SEIRS dates back to the year 2013. In this contribution, Law et al. used heavily doped InAs to tailor

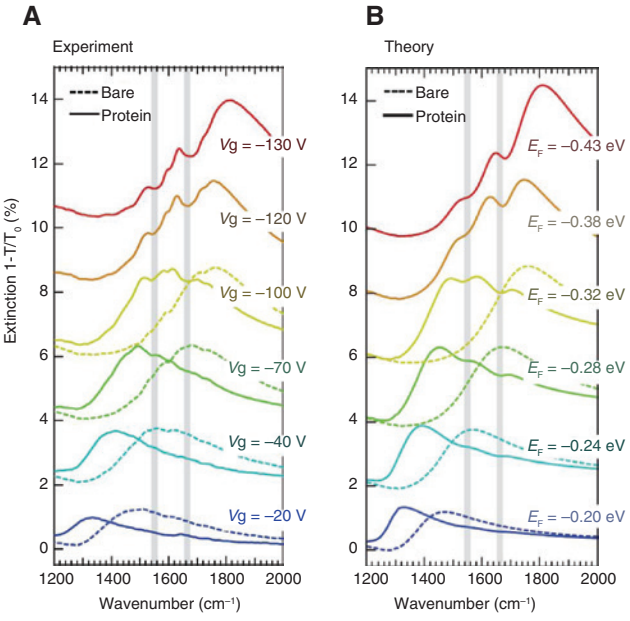

Figure 22: (A) Extinction spectra of the graphene nanoribbon array (W = 30 nm, P = 80 nm) for bias voltages *Vg* from –20 V to –130 V before (dashed curves) and after (solid curves) protein bilayer formation. Extinction is calculated as the relative difference in transmission between regions with (T) and without (T_0) graphene nanoribbons. Gray vertical strips indicate amide I and II vibrational bands of the protein. (B) Analytic calculation of the extinction spectra after fitting graphene and protein parameters to reproduce experimental data. Adapted with permission from Ref. [144].

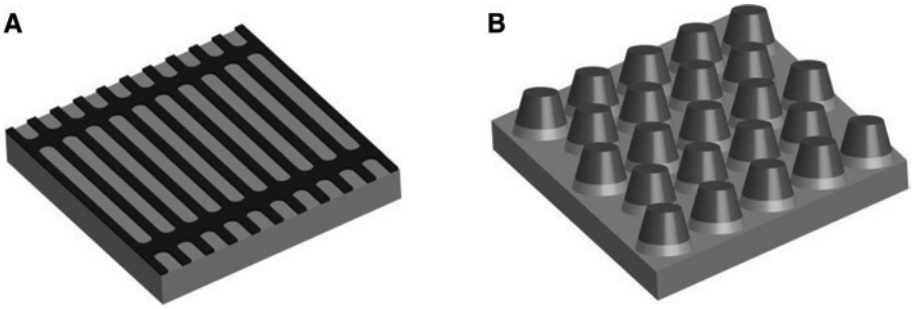

Figure 23: Two non-metal-based substrates for SEIRS.

plasmonic structures out of this material by nanosphere lithography [147]. From this fabrication method, disks (or nanopillars, Figure 23B) with sloped sidewalls ordered in a hexagonal lattice with distances much smaller than the wavelength result. Disks of three different diameters (165, 200 and 215 nm) and two different doping levels (resulting in plasma frequencies of 5.5 and 6.2 μm) were fabricated. Using a diameter of 200 nm and InAs with a plasma frequency of 6.2 μm, a good overlap of the plasmon resonance of the disks with the four PMMA vibrations between 750 and 850 cm^{-1} was achieved. The authors applied a 50 nm-thick PMMA layer as analyte and accomplished reflectance signals of somewhat less than 1% for the two medium strength PMMA vibrations at 752 and 842 cm^{-1}. The spectra were not noise-free despite the 4000 scans that were co-added per measurement. Usage of optimized structures instead of those resulting from nanosphere lithography might be able to improve this result.

A strongly related material, namely, highly-doped InAsSb was employed to prepare nanogratings for use in SEIRS [148]. The authors tuned the width and height of the gratings to adjust the corresponding plasmon resonance to the wavelength of 10 μm. At that wavelength, FDTD simulations predict a near-field enhancement $|E|/|E_0|$ of 170. The authors used a 200 nm-thick PMMA film, and its comparably weak resonances at 10.1 μm (990 cm^{-1}) and 10.35 μm (966 cm^{-1}) to test the performance and achieved an absorption signal of about 1% for the stronger mode at 10.1 μm in spectra with comparably good S/N.

Abb et al. [149] suggested the use of a transparent conducting oxide (TCO), indium tin oxide (ITO), as plasmonic material. In a very comprehensive study, they investigated arrays of mono- and dimers of linear nanoantennas of different lengths and different distances perpendicular to the long axis of the antennas and compared the results with that of equally shaped, spaced, and dimensioned antennas made out of gold. For dimer nanorod antennas with a gap of 50 nm, FEM calculations predict a near-field enhancement $|E|/|E_0|$ of about 190 at 1720 cm^{-1}. To test the performance, the authors used a 50 nm-thick PMMA layer as analyte and achieved transmittance signals of up to 8% for the strong C=O stretching vibration, which was about half of what could be gained from the gold nanoantenna arrays for lateral distances as small as 100 nm for ITO and 90 nm for gold (the spectra were comparably noisy; 100 scans were averaged per measurement). In evaluating these results, one has to keep in mind that such small distances perpendicular to the long axis lead to extreme interactions by scattering in the case of the gold nanoantennas, while these interactions are much smaller for ITO due to the much stronger spatial confinement of the plasmons.

Another semiconducting material with some promise for SEIRS is germanium, a material of high importance when it is undoped concerning its use in attenuated total reflection as incidence medium. To support plasmon resonances, it also needs to be highly doped and can then be used in spectral ranges up to 2500 cm^{-1}, which means that H-C-, H-N-, and H-O-stretching vibrations are out of reach [150]. Baldassarre et al. used it in the form of arrays of monomers and dimers of linear nanoantennas on Si, tuned to have resonances at 500 cm^{-1} (hotspots at the Si/Ge interface) and 900 cm^{-1} (hotspots at upper antenna edges). The latter resonance was employed to enhance the spectral features of the fairly strong Si-C vibration of a 40 nm-thick film of polydimethylsiloxane (PDMS) located at 800 cm^{-1}. The difference between the plasmon resonance wavenumber and the molecular vibration wavenumber may explain the fact that only a reflectance signal of about 0.5% could be achieved, which corresponds to a simulated maximum near-field intensity enhancement $|E|^2/|E_0|^2$ of about 70. The spectra showed a medium S/N.

A further TCO that can be used as a plasmonic material in the infrared is zinc oxide. From alternating layers of zinc oxide and gallium-doped zinc oxide (GZO) on Si, Kim et al. prepared nanopillars with sloped sidewalls in a cubic

lattice (ZnO/GZO/ZnO/GZO/Si substrate) [151]. The thickness of the ZnO layers amounted to 40 nm and that of the GZO layers to 120 nm. To benchmark the properties of the MIM structures (the top ZnO structure does not influence the optical properties) also pure GZO columns of the same height and dimensions were fabricated. The latter lack the plasmon resonance confined mostly within the ZnO sandwiched between the GZO layers. This resonance occurred between about 3.3 and 5 μm. The resonance wavelength is highly scalable with the diameter of the columns (in this case, 500 to 900 nm), but the columns also feature a plasmon resonance at about 2.2 μm that does nearly not vary with the diameter. To evaluate the performance of the substrate, the author used ODT, which does not seem to form monolayer on the structures, but instead forms films of about 20 nm thickness. The reflectance signal of the asymmetric CH_2 vibration of the ODT layer on columns with 500 nm diameter showed with about 4% in transmittance twice the signal of ODT on a substrate without any structure. About the same signal of 4% resulted from ODT on substrates with pure GZO columns. Changing the diameter of the columns to 700 and 900 nm resulted in a signal of about 6% and 7%, respectively. The spectra had a medium S/N.

GZO was also used as a plasmonic material in hexagonal bowtie structures fabricated by nanosphere lithography [152]. The authors investigated structures prepared using different sphere diameters and doping levels. The very broad plasmon resonance of these structures could be found between 3 and 5 μm. The performance of two of these structures was tested with a 50 nm-thick PMMA film, and a twofold enhancement of the transmittance signal was found for the C-H-stretching vibrations and a 1.4-fold enhancement for the C=O-stretching vibration if the plasmon was correspondingly tuned. The spectra displayed a good S/N.

Overall, it seems that most of the used semiconducting materials, so far, have plasma frequencies that render them less suitable for practical use in SEIRS. Again, the frequent use of comparably thick films to evaluate the SEIRS performance is somewhat puzzling. In particular, the reason for using semiconducting materials is the possibility to generate strongly bound plasmons, which should be particularly useful for monolayer applications.

4 Conclusion and outlook

Overall, there exists a multitude of very interesting and promising array structures for surface-enhanced infrared spectroscopy in the literature. For arrays of linear nanoantennas, a signal enhancement factor of about 10^4 to 10^5 can be considered as valid, which leads to overall reflectance or transmittance signals that can be detected with common lab equipment and sufficient S/N ratio. Overall, these signals may be an order of magnitude lower than those of metal island substrates. However, in particular, as soon as analyte molecules can be bound to the hotspots in a targeted manner, the higher local signal-enhancement factor of the array structures will show their inherent advantages. The benefits of arrays built of other shapes of nanoantennas like asymmetric split-ring resonators, crosses, etc., are generally hard to evaluate, mostly as the provided enhancement factors use unclear reference measurements or because signal-enhancement factors have not been determined at all. Therefore, a reevaluation would be advised and worthwhile. Compared to arrays of nanoantennas, arrays of inverse structures like slits have several benefits. Despite the lower maximum local near-field enhancement, the volume-averaged near-field enhancement leads to stronger signals. In addition, the near-field intensity distribution within holes render them ideal candidates to detect analytes by binding them to capture molecules, as analyte and electric fields can be concentrated in the same volume. Likewise, perfect absorber structures might be helpful to overcome, at least partly, the strong diffractive coupling between particles, thereby, enabling not only stronger near-field enhancements but also somewhat higher surface coverage. In principle, higher surface coverage could also be realized by the use of structures made out of doped semiconductors or graphene. For most of the semiconducting materials employed so far, however, even strong doping leads to plasma frequencies, which are too low to be of interest for SEIRS. For future developments, in particular, 3D structures could be of great benefit, as they promise stronger field enhancements due to their monopole structure and an enhanced interaction between particles. Here, targeted delivery of analytes to the hotspots will even be more challenging, as these are all-metal structures.

A general challenge is to increase near-field enhancement factor and signal not only for one particular spectral region, but for all spectral regions that are of interest for mid-infrared sensing. First and promising steps in this direction have already been undertaken, and we hope for more progress in this direction in the next years.

Acknowledgments: Financial support of the EU, the "Thüringer Ministerium für Wirtschaft, Wissenschaft und Digitale Gesellschaft", the "Thüringer Aufbaubank", the Federal Ministry of Education and Research, Germany

(BMBF), the German Science Foundation, the Fonds der Chemischen Industrie, and the Carl-Zeiss Foundation are greatly acknowledged.

References

[1] Hartstein A, Kirtley JR, Tsang JC. Enhancement of the infrared absorption from molecular monolayers with thin metal overlayers. Phys Rev Lett 1980;45:201–4.
[2] Eischens RP, Pliskin WA. The infrared spectra of adsorbed molecules. In: Eley WGFVIKDD, Paul BW, eds. Advances in catalysis, San Diego, CA, Academic Press; 1958, p. 1–56.
[3] Bradshaw AM, Pritchard J. Infra-red spectra of carbon monoxide on evaporated nickel films. Surf Sci 1969;17:372–86.
[4] Aroca RF, Ross DJ, Domingo C. Surface-enhanced infrared spectroscopy. Appl Spectrosc. 2004;58:324A–38A.
[5] Osawa M. Surface-enhanced infrared absorption. Near-Field Opt Surf Plasmon Polaritons 2001;81:163–87.
[6] Ataka K, Heberle J. Biochemical applications of surface-enhanced infrared absorption spectroscopy. Anal Bioanal Chem 2007;388:47–54.
[7] Osawa M, Ataka K-I, Yoshii K, Nishikawa Y. Surface-enhanced infrared spectroscopy: the origin of the absorption enhancement and band selection rule in the infrared spectra of molecules adsorbed on fine metal particles. Appl Spectrosc 1993;47:1497–502.
[8] Johnson E, Aroca R. Surface-enhanced infrared spectroscopy of monolayers. J Phys Chem 1995;99:9325–30.
[9] Röseler A, Korte EH. Surface enhanced infrared absorption observed with attenuated total reflection (ATR-SEIRA): modeling the optical response. Fresenius J Anal Chem 1998;362:51–7.
[10] Ross D, Aroca R. Effective medium theories in surface enhanced infrared spectroscopy: the pentacene example. J Chem Phys 2002;117:8095–103.
[11] Priebe A, Sinther M, Fahsold G, Pucci A. The correlation between film thickness and adsorbate line shape in surface enhanced infrared absorption. J Chem Phys 2003;119:4887–90.
[12] Bjerke AE, Griffiths PR, Theiss W. Surface-enhanced infrared absorption of co on platinized platinum. Anal Chem 1999;71:1967–74.
[13] Chettiar UK, Nyga P, Thoreson MD, Kildishev AV, Drachev VP, Shalaev VM. FDTD modeling of realistic semicontinuous metal films. Appl Phys B 2010;100:159–68.
[14] Osawa M, Ikeda M. Surface-enhanced infrared absorption of p-nitrobenzoic acid deposited on silver island films: contributions of electromagnetic and chemical mechanisms. J Phys Chem 1991;95:9914–9.
[15] Dominik E, Tadaaki N, Tomonobu N, Masakazu A. Precisely controlled fabrication of a highly sensitive Au sensor film for surface enhanced spectroscopy. Jpn J Appl Phys 46;2007:L1222.
[16] Enders D, Nagao T, Pucci A, Nakayama T, Aono M. Surface-enhanced ATR-IR spectroscopy with interface-grown plasmonic gold-island films near the percolation threshold. Phys Chem Chem Phys PCCP 2011;13:4935–41.
[17] Heaps DA, Griffiths PR. Band shapes in the infrared spectra of thin organic films on metal nanoparticles. Vib Spectrosc 2006;42:45–50.
[18] Jahn M, Patze S, Hidi IJ, et al. Plasmonic nanostructures for surface enhanced spectroscopic methods. Analyst 2016;141:756–93.
[19] Van Hardeveld R, Van Montfoort A. Infrared spectra of nitrogen adsorbed on nickel-on-aerosil catalysts. Surf Sci 1969;17:90–124.
[20] Boujday S, de la Chapelle ML, Srajer J, Knoll W. Enhanced vibrational spectroscopies as tools for small molecule biosensing. Sensors 2015;15:21239–64.
[21] Aroca R. Surface-enhanced vibrational spectroscopy. Hoboken, NJ: Wiley; 2006.
[22] Bedford EE, Boujday S, Pradier CM, Gu FX. Nanostructured and spiky gold in biomolecule detection: improving binding efficiencies and enhancing optical signals. RSC Adv 2015;5:16461–75.
[23] Krauth O, Fahsold G, Pucci A. Asymmetric line shapes and surface enhanced infrared absorption of CO adsorbed on thin iron films on MgO(001). J Chem Phys 1999;110:3113–7.
[24] Langreth DC. Energy transfer at surfaces: asymmetric line shapes and the electron-hole-pair mechanism. Phys Rev Lett 1985;54:126–9.
[25] Giannini V, Francescato Y, Amrania H, Phillips CC, Maier SA. Fano resonances in nanoscale plasmonic systems: a parameter-free modeling approach. Nano Lett 2011;11:2835–40.
[26] Adato R, Artar A, Erramilli S, Altug H. Engineered absorption enhancement and induced transparency in coupled molecular and plasmonic resonator systems. Nano Lett 2013;13:2584–91.
[27] Neuman T, Huck C, Vogt J, et al. Importance of plasmonic scattering for an optimal enhancement of vibrational absorption in SEIRA with linear metallic antennas. J Phys Chem C 2015;119:26652–62.
[28] Vogt J, Huck C, Neubrech F, Toma A, Gerbert D, Pucci A. Impact of the plasmonic near- and far-field resonance-energy shift on the enhancement of infrared vibrational signals. Phys Chem Chem Phys 2015;17:21169–75.
[29] Alonso-Gonzalez P, Albella P, Neubrech F, et al. Experimental verification of the spectral shift between near- and far-field peak intensities of plasmonic infrared nanoantennas. Phys Rev Lett 2013;110:203902.
[30] Hayashi S, Kanamori H. Infrared study of surface phonon modes in α-Fe2O3 microcrystals. J Phys C Solid State 1980;13:1529.
[31] Novotny L, Hecht B. Principles of nano-optics. Cambridge, Cambridge University Press; 2012.
[32] Gersten J, Nitzan A. Electromagnetic theory of enhanced Raman scattering by molecules adsorbed on rough surfaces. J Chem Phys 1980;73:3023–37.
[33] Hartschuh A. Tip-enhanced optical spectroscopy. Philos Trans A Math Phys Eng Sci 2004;362:807–19.
[34] Knoll B, Keilmann F. Near-field probing of vibrational absorption for chemical microscopy. Nature 1999;399:134–7.
[35] Taubner T, Hillenbrand R, Keilmann F. Nanoscale polymer recognition by spectral signature in scattering infrared near-field microscopy. Appl Phys Lett 2004;85:5064–6.
[36] Le F, Brandl DW, Urzhumov YA, et al. Metallic nanoparticle arrays: a common substrate for both surface-enhanced Raman scattering and surface-enhanced infrared absorption. ACS Nano 2008;2:707–18.
[37] Shimada T, Nakashima H, Kumagai Y, et al. What is the key structural parameter for infrared absorption enhancement on nanostructures? J Phys Chem C 2016;120:534–41.

[38] Larmour IA, Graham D. Surface enhanced optical spectroscopies for bioanalysis. Analyst 2011;136:3831–53.
[39] Kleinman SL, Frontiera RR, Henry A-I, Dieringer JA, Van Duyne RP. Creating, characterizing, and controlling chemistry with SERS hot spots. Phys Chem Chem Phys 2013;15:21–36.
[40] Dregely D, Neubrech F, Duan H, Vogelgesang R, Giessen H. Vibrational near-field mapping of planar and buried three-dimensional plasmonic nanostructures. Nat Commun 2013;4:2237.
[41] Weber D, Albella P, Alonso-González P, et al. Longitudinal and transverse coupling in infrared gold nanoantenna arrays: long range versus short range interaction regimes. Opt Express 2011;19:15047–61.
[42] Lahiri B, Holland G, Aksyuk V, Centrone A. Nanoscale imaging of plasmonic hot spots and dark modes with the photothermal-induced resonance technique. Nano Lett 2013;13:3218–24.
[43] Tsukerman I. Computational methods for nanoscale applications: particles, plasmons and waves. New York, NY, Springer; 2007.
[44] Obayya S. Computational photonics. Hoboken, NJ, Wiley; 2011.
[45] Rylander T, Ingelström P, Bondeson A. Computational electromagnetics. New York, NY, Springer; 2012.
[46] Mayerhöfer TG, Mutschke H, Popp J. Employing theories far beyond their limits – the case of the (Boguer-) Beer–Lambert law. Chemphyschem 2016;17:1948–55.
[47] Ayas S, Bakan G, Ozgur E, Celebi K, Dana A. Universal infrared absorption spectroscopy using uniform electromagnetic enhancement. ACS Photonics 2016;3:337–42.
[48] Hansen WN. Expanded formulas for attenuated total reflection and the derivation of absorption rules for single and multiple ATR spectrometer cells. Spectrochim Acta 1965;21:815–33.
[49] Chalmers JM, Griffiths PR. Handbook of vibrational spectroscopy. New York, NY, Wiley; 2002.
[50] Kim YT, Bard AJ. Imaging and etching of self-assembled n-octadecanethiol layers on gold with the scanning tunneling microscope. Langmuir 1992;8:1096–102.
[51] Porter MD, Bright TB, Allara DL, Chidsey CED. Spontaneously organized molecular assemblies. 4. Structural characterization of n-alkyl thiol monolayers on gold by optical ellipsometry, infrared spectroscopy, and electrochemistry. J Am Chem Soc 1987;109:3559–68.
[52] Zolotarev VM, Volchek BZ, Vlasova EN. Optical constants of industrial polymers in the IR region. Opt Spectrosc 2006;101:716–23.
[53] Graf RT, Koenig JL, Ishida H. Optical constant determination of thin polymer films in the infrared. Appl Spectrosc 1985;39:405–8.
[54] Maß TWW, Taubner T. Incident angle-tuning of infrared antenna array resonances for molecular sensing. ACS Photonics 2015;2:1498–504.
[55] Parikh AN, Allara DL. Quantitative determination of molecular structure in multilayered thin films of biaxial and lower symmetry from photon spectroscopies. I. Reflection infrared vibrational spectroscopy. J Chem Phys 1992;96:927.
[56] Brown LV, Yang X, Zhao K, Zheng BY, Nordlander P, Halas NJ. Fan-shaped gold nanoantennas above reflective substrates for surface-enhanced infrared absorption (SEIRA). Nano Lett 2015;15:1272–80.
[57] Berreman DW. Infrared absorption at longitudinal optic frequency in cubic crystal films. Phys Rev 1963;130:2193–8.
[58] Enders D, Pucci A. Surface enhanced infrared absorption of octadecanethiol on wet-chemically prepared Au nanoparticle films. Appl Phys Lett 2006;88:184104.
[59] Spitzer W, Kleinman D. Infrared lattice bands of quartz. Phys Rev 1961;121:1324–35.
[60] Adato R, Yanik AA, Amsden JJ, et al. Ultra-sensitive vibrational spectroscopy of protein monolayers with plasmonic nanoantenna arrays, Proc Natl Acad Sci USA 2009;106:19227–32.
[61] Mayerhofer TG, Ivanovski V, Popp J. Dispersion analysis with inverse dielectric function modelling. Spectrochim Acta A Mol Biomol Spectrosc 2016;168:212–7.
[62] Allara DL, Parikh AN, Rondelez F. Evidence for a unique chain organization in long chain silane monolayers deposited on two widely different solid substrates. Langmuir 1995;11:2357–60.
[63] Tolstoy VP, Chernyshova I, Skryshevsky VA. Handbook of infrared spectroscopy of ultrathin films. Hoboken, NJ, Wiley; 2003.
[64] Solonenko D, Gordan OD, Milekhin A, Panholzer M, Hingerl K, Zahn DRT. Interference-enhanced Raman scattering of F16CuPc thin films. J Phys D Appl Phys 2016;49:115502.
[65] Limaj O, Etezadi D, Wittenberg NJ, et al. Infrared plasmonic biosensor for real-time and label-free monitoring of lipid membranes. Nano Lett 2016;16:1502–8.
[66] Neubrech F, Beck S, Glaser T, Hentschel M, Giessen H, Pucci A. Spatial extent of plasmonic enhancement of vibrational signals in the infrared. ACS Nano 2014;8:6250–8.
[67] Jensen TR, Van Duyne RP, Johnson SA, Maroni VA. Surface-enhanced infrared spectroscopy: a comparison of metal island films with discrete and nondiscrete surface plasmons. Appl Spectrosc 2000;54:371–7.
[68] Crozier KB, Sundaramurthy A, Kino GS, Quate CF. Optical antennas: resonators for local field enhancement. J Appl Phys 2003;94:4632–42.
[69] Neubrech F, Pucci A, Cornelius T, Karim S, García-Etxarri A, Aizpurua J. Resonant plasmonic and vibrational coupling in a tailored nanoantenna for infrared detection. Phys Rev Lett 2008;101:157403.
[70] Cerjan B, Yang X, Nordlander P, Halas NJ. Asymmetric aluminum antennas for self-calibrating surface-enhanced infrared absorption spectroscopy. ACS Photonics 2016;3:354–60.
[71] Puscasu I, Schaich WL, Boreman GD. Modeling parameters for the spectral behavior of infrared frequency-selective surfaces. Appl Opt 2001;40:118–24.
[72] Puscasu I, Schaich W, Boreman GD. Resonant enhancement of emission and absorption using frequency selective surfaces in the infrared. Infrared Phys Technol 2002;43:101–7.
[73] Weber D, Katzmann J, Neubrech F, Härtling T, Pucci A. Spectral tuning of IR-resonant nanoantennas by nanogap engineering. Opt Mater Express 2011;1:1301–6.
[74] Liberman V, Adato R, Mertiri A, et al. Angle-and polarization-dependent collective excitation of plasmonic nanoarrays for surface enhanced infrared spectroscopy. Opt Express 2011;19:11202–12.
[75] Liberman V, Adato R, Jeys TH, Saar BG, Erramilli S, Altug H. Rational design and optimization of plasmonic nanoarrays for surface enhanced infrared spectroscopy. Opt Express 2012;20:11953–67.
[76] Hoffmann JM, Yin X, Richter J, Hartung A, Maß TWW, Taubner T. Low-cost infrared resonant structures for surface-enhanced infrared absorption spectroscopy in the fingerprint region from 3 to 13 μm. J Phys Chem C 2013;117:11311–6.

[77] Pucci A, Neubrech F, Weber D, Hong S, Toury T, de la Chapelle ML. Surface enhanced infrared spectroscopy using gold nanoantennas. Phys Status Solidi (b) 2010;247:2071–4.
[78] Neubrech F, Weber D, Katzmann J, et al. Infrared optical properties of nanoantenna dimers with photochemically narrowed gaps in the 5 nm regime. ACS Nano 2012;6:7326–32.
[79] Huck C, Neubrech F, Vogt J, et al. Surface-enhanced infrared spectroscopy using nanometer-sized gaps. ACS Nano 2014;8:4908–14.
[80] Aksu S, Cetin AE, Adato R, Altug H. Plasmonically enhanced vibrational biospectroscopy using low-cost infrared antenna arrays by nanostencil lithography. Adv Opt Mater 2013;1:798–803.
[81] Bagheri S, Weber K, Gissibl T, Weiss T, Neubrech F, Giessen H. Fabrication of square-centimeter plasmonic nanoantenna arrays by femtosecond direct laser writing lithography: effects of collective excitations on SEIRA enhancement. ACS Photonics 2015;2:779–86.
[82] Bochterle J, Neubrech F, Nagao T, Pucci A. Angstrom-scale distance dependence of antenna-enhanced vibrational signals. ACS Nano 2012;6:10917–23.
[83] Alonso-Gonzalez P, Albella P, Schnell M, et al. Resolving the electromagnetic mechanism of surface-enhanced light scattering at single hot spots. Nat Commun 2012;3:684.
[84] Neubrech F, Weber D, Enders D, Nagao T, Pucci A. Antenna sensing of surface phonon polaritons. J Phys Chem C 2010;114:7299–301.
[85] Mayerhöfer TG, Shen Z, Leonova E, Edén M, Kriltz A, Popp J. Consolidated silica glass from nanoparticles. J Solid State Chem 2008;181:2442–7.
[86] Cetin AE, Etezadi D, Altug H. Accessible nearfields by nanoantennas on nanopedestals for ultrasensitive vibrational spectroscopy. Adv Opt Mater 2014;2:866–72.
[87] Huck C, Toma A, Neubrech F, et al. Gold nanoantennas on a pedestal for plasmonic enhancement in the infrared. ACS Photonics 2015;2:497–505.
[88] D'Andrea C, Bochterle J, Toma A, et al. Optical nanoantennas for multiband surface-enhanced infrared and raman spectroscopy. ACS Nano 2013;7:3522–31.
[89] Reininghaus M, Wortmann D, Cao Z, Hoffmann JM, Taubner T. Fabrication and spectral tuning of standing gold infrared antennas using single fs-laser pulses. Opt Express 2013;21:32176–83.
[90] Malerba M, Alabastri A, Miele E, et al. 3D vertical nanostructures for enhanced infrared plasmonics. Sci Rep 2015;5:16436.
[91] Zilio P, Malerba M, Toma A, Zaccaria RP, Jacassi A, De Angelis F. Hybridization in three dimensions: a novel route toward plasmonic metamolecules. Nano Lett 2015;15:5200–7.
[92] Adato R, Altug H. In-situ ultra-sensitive infrared absorption spectroscopy of biomolecule interactions in real time with plasmonic nanoantennas. Nat Commun 2013;4:2154.
[93] Wang T, Nguyen VH, Buchenauer A, Schnakenberg U, Taubner T. Surface enhanced infrared spectroscopy with gold strip gratings. Opt Express 2013;21:9005–10.
[94] Petefish JW, Hillier AC. Angle-tunable enhanced infrared reflection absorption spectroscopy via grating-coupled surface plasmon resonance. Anal Chem 2014;86:2610–7.
[95] Petefish JW, Hillier AC. Multipitched diffraction gratings for surface plasmon resonance-enhanced infrared reflection absorption spectroscopy. Anal Chem 2015;87:10862–70.
[96] Brown LV, Zhao K, King N, Sobhani H, Nordlander P, Halas NJ. Surface-enhanced infrared absorption using individual cross antennas tailored to chemical moieties. J Am Chem Soc 2013;135:3688–95.
[97] Bagheri S, Giessen H, Neubrech F. Large-area antenna-assisted SEIRA substrates by laser interference lithography. Adv Opt Mater 2014;2:1050–6.
[98] Hoffmann JM, Janssen H, Chigrin DN, Taubner T. Enhanced infrared spectroscopy using small-gap antennas prepared with two-step evaporation nanosphere lithography. Opt Express 2014;22:14425–32.
[99] Aouani H, Šípová H, Rahmani M, et al. Ultrasensitive broadband probing of molecular vibrational modes with multifrequency optical antennas. ACS Nano 2013;7:669–75.
[100] Bukasov R, Shumaker-Parry JS. Silver nanocrescents with infrared plasmonic properties as tunable substrates for surface enhanced infrared absorption spectroscopy. Anal Chem 2009;81:4531–35.
[101] Cooper CT, Rodriguez M, Blair S, Shumaker-Parry JS. Mid-infrared localized plasmons through structural control of gold and silver nanocrescents. J Phys Chem C 2015;119:11826–32.
[102] Cubukcu E, Zhang S, Park Y-S, Bartal G, Zhang X. Split ring resonator sensors for infrared detection of single molecular monolayers. Appl Phys Lett 2009;95:043113.
[103] Cataldo S, Zhao J, Neubrech F, et al. Hole-mask colloidal nanolithography for large-area low-cost metamaterials and antenna-assisted surface-enhanced infrared absorption substrates. ACS Nano 2012;6:979–85.
[104] Lahiri B, Khokhar AZ, De La Rue RM, McMeekin SG, Johnson NP. Asymmetric split ring resonators for optical sensing of organic materials. Opt Express 2009;17:1107–15.
[105] Lahiri B, McMeekin SG, De La Rue RM, Johnson NP. Resonance hybridization in nanoantenna arrays based on asymmetric split-ring resonators. Appl Phys Lett 2011;98:153116.
[106] Aksyuk V, Lahiri B, Holland G, Centrone A. Near-field asymmetries in plasmonic resonators. Nanoscale 2015;7:3634–44.
[107] Chae J, Lahiri B, Kohoutek J, Holland G, Lezec H, Centrone A. Metal-dielectric-metal resonators with deep subwavelength dielectric layers increase the near-field SEIRA enhancement. Opt Express 2015;23:25912–22.
[108] Chae J, Lahiri B, Centrone A. Engineering near-field SEIRA enhancements in plasmonic resonators. ACS Photonics 2016;3:87–95.
[109] Pryce IM, Aydin K, Kelaita YA, Briggs RM, Atwater HA. Highly strained compliant optical metamaterials with large frequency tunability. Nano Lett 2010;10:4222–7.
[110] Pryce IM, Kelaita YA, Aydin K, Atwater HA. Compliant metamaterials for resonantly enhanced infrared absorption spectroscopy and refractive index sensing. ACS Nano 2011;5:8167–74.
[111] Wu C, Khanikaev AB, Adato R, et al. Fano-resonant asymmetric metamaterials for ultrasensitive spectroscopy and identification of molecular monolayers. Nat Mater 2012;11:69–75.
[112] Shelton DJ, Brener I, Ginn JC, et al. Strong coupling between nanoscale metamaterials and phonons. Nano Lett 2011;11:2104–8.
[113] Huck C, Vogt J, Neuman T, et al. Strong coupling between phonon-polaritons and plasmonic nanorods. Opt Express 2016;24:25528–39.

[114] Galeener F, Leadbetter A, Stringfellow M. Comparison of the neutron, Raman, and infrared vibrational spectra of vitreous SiO_{2}, GeO_{2}, and BeF_{2}. Phys Rev B 1983;27:1052–78.
[115] Kirk C. Quantitative analysis of the effect of disorder-induced mode coupling on infrared absorption in silica. Phys Rev B 1988;38:1255–73.
[116] Mayerhöfer TG, Dunken HH, Keding R, Rüssel C. Interpretation and modeling of IR-reflectance spectra of glasses considering medium range order. J Non Cryst Solids 2004;333:172–81.
[117] Zentgraf T, Meyrath TP, Seidel A, et al. Babinet's principle for optical frequency metamaterials and nanoantennas. Phys Rev B 2007;76:033407.
[118] Williams SM, Stafford AD, Rodriguez KR, Rogers TM, Coe JV. Accessing surface plasmons with Ni microarrays for enhanced IR absorption by monolayers. J Phys Chem B 2003;107:11871–9.
[119] Ebbesen TW, Lezec HJ, Ghaemi HF, Thio T, Wolff PA. Extraordinary optical transmission through sub-wavelength hole arrays. Nature 1998;391:667–9.
[120] Williams SM, Rodriguez KR, Teeters-Kennedy S, et al. Use of the extraordinary infrared transmission of metallic subwavelength arrays to study the catalyzed reaction of methanol to formaldehyde on copper oxide. J Phys Chem B 2004;108:11833–7.
[121] Rodriguez KR, Shah S, Williams SM, Teeters-Kennedy S, Coe JV. Enhanced infrared absorption spectra of self-assembled alkanethiol monolayers using the extraordinary infrared transmission of metallic arrays of subwavelength apertures. J Chem Phys 2004;121:8671–5.
[122] Coe JV, Williams SM, Rodriguez KR, Teeters-Kennedy S, Sudnitsyn A, Hrovat F. Extraordinary IR transmission with metallic arrays of subwavelength holes. Anal Chem 2006;78:1384–90.
[123] Teeters-Kennedy SM, Rodriguez KR, Rogers TM, et al. Controlling the passage of light through metal microchannels by nanocoatings of phospholipids. J Phys Chem B 2006;110:21719–27.
[124] Rodriguez KR, Tian H, Heer JM, Teeters-Kennedy S, Coe JV. Interaction of an infrared surface plasmon with an excited molecular vibration. J Chem Phys 2007;126:151101.
[125] Limaj O, D'Apuzzo F, Di Gaspare A, et al. Mid-infrared surface plasmon polariton sensors resonant with the vibrational modes of phospholipid layers. J Phys Chem C 2013;117:19119–26.
[126] Nishijima Y, Nigorinuma H, Rosa L, Juodkazis S. Selective enhancement of infrared absorption with metal hole arrays. Opt Mater Express 2012;2:1367–77.
[127] Nishijima Y, Adachi Y, Rosa L, Juodkazis S. Augmented sensitivity of an IR-absorption gas sensor employing a metal hole array. Opt Mater Express 2013;3:968.
[128] Huck C, Vogt J, Sendner M, Hengstler D, Neubrech F, Pucci A. Plasmonic enhancement of infrared vibrational signals: nanoslits versus nanorods. ACS Photonics 2015;2:1489–97.
[129] Cetin AE, Turkmen M, Aksu S, Etezadi D, Altug H. Multi-resonant compact nanoaperture with accessible large nearfields. Appl Phys B 2014;118:29–38.
[130] Cheng F, Yang X, Gao J. Ultrasensitive detection and characterization of molecules with infrared plasmonic metamaterials. Sci Rep 2015;5:14327.
[131] Landy NI, Sajuyigbe S, Mock JJ, Smith DR, Padilla WJ. Perfect metamaterial absorber. Phys Rev Lett 2008;100:207402.
[132] Liu X, Starr T, Starr AF, Padilla WJ. Infrared spatial and frequency selective metamaterial with near-unity absorbance. Phys Rev Lett 2010;104:207403.
[133] Chen K, Adato R, Altug H. Dual-band perfect absorber for multispectral plasmon-enhanced infrared spectroscopy. ACS Nano 2012;6:7998–8006.
[134] Cetin AE, Korkmaz S, Durmaz H, et al. Quantification of multiple molecular fingerprints by dual-resonant perfect absorber. Adv Opt Mater 2016;4:1274–80.
[135] Li Y, Su L, Shou C, Yu C, Deng J, Fang Y. Surface-enhanced molecular spectroscopy (SEMS) based on perfect-absorber metamaterials in the mid-infrared. Sci Rep 2013;3:2865.
[136] Chen K, Dao TD, Ishii S, Aono M, Nagao T. Infrared aluminum metamaterial perfect absorbers for plasmon-enhanced infrared spectroscopy. Adv Funct Mater 2015;25:6637–43.
[137] Srajer J, Schwaighofer A, Ramer G, et al. Double-layered nanoparticle stacks for surface enhanced infrared absorption spectroscopy. Nanoscale 2014;6:127–31.
[138] Chen X, Ciraci C, Smith DR, Oh SH. Nanogap-enhanced infrared spectroscopy with template-stripped wafer-scale arrays of buried plasmonic cavities. Nano Lett 2015;15:107–13.
[139] Ishikawa A, Tanaka T. Metamaterial absorbers for infrared detection of molecular self-assembled monolayers. Sci Rep 2015;5:12570.
[140] Mayerhöfer TG, Knipper R, Hübner U, et al. Ultra sensing by combining extraordinary optical transmission with perfect absorption. ACS Photonics 2015;2:1567–75.
[141] Xiong X, Jiang SC, Hu YH, Peng RW, Wang M. Structured metal film as a perfect absorber. Adv Mater 2013;25:3994–4000.
[142] Chevalier P, Bouchon P, Greffet J-J, Pelouard J-L, Haïdar R, Pardo F. Giant field enhancement in electromagnetic Helmholtz nanoantenna. Phys Rev B 2014;90:195412.
[143] Vasić B, Isić G, Gajić R. Localized surface plasmon resonances in graphene ribbon arrays for sensing of dielectric environment at infrared frequencies. J Appl Phys 2013;113:013110.
[144] Rodrigo D, Limaj O, Janner D, et al. Mid-infrared plasmonic biosensing with grapheme. Science 2015;349:165–8.
[145] Farmer DB, Avouris P, Li Y, Heinz TF, Han S-J. Ultrasensitive plasmonic detection of molecules with graphene. ACS Photonics 2016;3:553–7.
[146] Marini A, Silveiro I, García de Abajo FJ. Molecular sensing with tunable graphene plasmons. ACS Photonics 2015;2:876–82.
[147] Law S, Yu L, Rosenberg A, Wasserman D. All-semiconductor plasmonic nanoantennas for infrared sensing. Nano Lett 2013;13:4569–74.
[148] Barho FB, Gonzalez-Posada F, Milla-Rodrigo M-J, Bomers M, Cerutti L, Taliercio T. All-semiconductor plasmonic gratings for biosensing applications in the mid-infrared spectral range. Opt Express 2016;24:16175–90.
[149] Abb M, Wang Y, Papasimakis N, de Groot CH, Muskens OL. Surface-enhanced infrared spectroscopy using metal oxide plasmonic antenna arrays. Nano Lett 2014;14:346–52.
[150] Baldassarre L, Sakat E, Frigerio J, et al. Midinfrared plasmon-enhanced spectroscopy with germanium antennas on silicon substrates. Nano Lett 2015;15:7225–31.
[151] Kim J, Dutta A, Memarzadeh B, Kildishev AV, Mosallaei H, Boltasseva A. Zinc oxide based plasmonic multilayer resonator: localized and gap surface plasmon in the infrared. ACS Photonics 2015;2:1224–30.
[152] Habeeb AA, Long H, Bao L, Wang K, Wang B, Lu P. Surface plasmonic resonances and enhanced IR spectra in GZO nanotriangle arrays. Mater Lett 2016;172:36–9.